

Article

Altered Brain Complexity in Women with Primary Dysmenorrhea: A Resting-State Magneto-Encephalography Study Using Multiscale Entropy Analysis

Intan Low ¹ , Po-Chih Kuo ² , Yu-Hsiang Liu ³, Cheng-Lin Tsai ¹, Hsiang-Tai Chao ⁴, Jen-Chuen Hsieh ^{3,5}, Li-Fen Chen ^{1,3,5,*} and Yong-Sheng Chen ^{2,6,*} 

¹ Institute of Biomedical Informatics, National Yang-Ming University, Taipei 11221, Taiwan; d40023003@ym.edu.tw (I.L.); f901107@ym.edu.tw (C.-L.T.)

² Department of Computer Science, National Chiao Tung University, Hsinchu 30010, Taiwan; kuopc@cs.nctu.edu.tw

³ Institute of Brain Science, National Yang-Ming University, Taipei 11221, Taiwan; r00261060@gmail.com (Y.-H.L.); jchsieh@ym.edu.tw (J.-C.H.)

⁴ Department of Obstetrics and Gynecology, Taipei Veterans General Hospital, Taipei 11217, Taiwan; htchao@vghtpe.gov.tw

⁵ Integrated Brain Research Unit, Department of Medical Research, Taipei Veterans General Hospital, Taipei 11217, Taiwan

⁶ Institute of Biomedical Engineering, National Chiao Tung University, Hsinchu 30010, Taiwan

* Correspondence: lfchen@ym.edu.tw (L.-F.C.); yschen@cs.nctu.edu.tw (Y.-S.C.); Tel.: +886-2-2826-7384 (L.-F.C.); +886-3-5131-316 (Y.-S.C.)

Received: 30 September 2017; Accepted: 6 December 2017; Published: 11 December 2017

Abstract: How chronic pain affects brain functions remains unclear. As a potential indicator, brain complexity estimated by entropy-based methods may be helpful for revealing the underlying neurophysiological mechanism of chronic pain. In this study, complexity features with multiple time scales and spectral features were extracted from resting-state magnetoencephalographic signals of 156 female participants with/without primary dysmenorrhea (PDM) during pain-free state. Revealed by multiscale sample entropy (MSE), PDM patients (PDMs) exhibited loss of brain complexity in regions associated with sensory, affective, and evaluative components of pain, including sensorimotor, limbic, and salience networks. Significant correlations between MSE values and psychological states (depression and anxiety) were found in PDMs, which may indicate specific nonlinear disturbances in limbic and default mode network circuits after long-term menstrual pain. These findings suggest that MSE is an important measure of brain complexity and is potentially applicable to future diagnosis of chronic pain.

Keywords: multiscale sample entropy; chronic pain; primary dysmenorrhea; complexity; magnetoencephalography; resting-state network

1. Introduction

Chronic pain, any continuous or recurrent pain lasting for more than three to six months [1,2], may cause reorganization of the central nervous system [3]. It is a worldwide public health problem associated with mildly increased mortality [4]. Primary dysmenorrhea (PDM), highly prevalent yet undertreated and affecting 40–90% of the reproductive-age females [5–7], is a pelvic pain during menstruation without identifiable structural lesion or anomaly in the internal female genital organs [8]. PDM is a good clinical model for studying chronic pain because of its natural “on” (painful) and “off” (pain-free) states. PDM patients (PDMs) suffer from long-term recurrent menstrual pain, lasting

for an extended period (8 to 72 h) during each menstrual cycle for years [9,10]. This highlights the uniqueness of long-term PDM, which comprises the experiences of visceral acute tonic pain during menstrual cramp and recurrent pain during each menstrual cycle over the course of reproductive age. Such long-term menstrual pain shapes their brains and changes the way they perceive, modulate, and react to pain, leading to reduced quality of life, various mental and physiological health problems such as pain catastrophizing, depression, anxiety, and sleep disorders [7,11,12], and high comorbidity with many functional pain disorders later in life [13,14]. Alterations in brain structures [15–18] and functions [13,19–26] in PDMs have been reported, albeit far too little attention has been paid to the changes of cortical dynamics in PDMs.

The brain encompasses both regular and irregular neuronal interactions. The former is often regarded as linear, predictable, synchronous, or oscillatory and the latter is regarded as nonlinear, unpredictable, asynchronous, or nonoscillatory [27]. The irregularity and unpredictability of brain activity can be regarded as neural complexity, which is related to the brain functions and the information processing between neurons [28,29]. However, up-to-now, neural activities in the brain are typically analyzed using linear approximations, such as power-spectrum or time-frequency analyses. It is noteworthy that nonlinear interactions are thought to be as important as, if not more important, and more sensitive than linear interactions in characterizing brain dynamics [30]. These interactions can be reflected by brief neuronal transients between synaptic reentrant loops and are embedded in time-series neurophysiological signals [31]. The complexity of brain signal patterns reveals the neurophysiological information [28,32]. Quantification of moment-to-moment temporal variability would provide a useful metric of brain dynamics [33], which may not be resolved by conventional spectral-based analysis. Entropy-based analysis, such as sample entropy [34], is a powerful tool to quantify complexity in nonlinear dynamics of neuronal activities.

The spatial and temporal scales of neurophysiological systems range from microscopic to macroscopic aspects [35]. Alterations at any scale of these aspects could challenge the normal/healthy brain functioning. Local neuronal populations constitute intra-regional and inter-regional functional brain networks, give rise to various physiological and psychological functions, and ultimately generate simple and complex human behaviors. Multiscale entropy (MSE) approach, which measures complexity or irregularity by calculating sample entropy over multiple time scales [36,37], provides additional information of temporal scales from neurophysiological time-varying signals. MSE has been applied in characterizing various types of neurophysiological signals [38,39], including electroencephalography (EEG) [40–50], event-related potentials [51–55], magnetoencephalography (MEG) [26,47,56–59], and functional magnetic resonance imaging (fMRI) data [28,33,49,60,61]. MEG, as a noninvasive neurophysiological measurement with superior temporal resolution (approximately 1 ms) and good spatial resolution (approximately 4~5 mm), possesses high sensitivity in capturing entropy changes of neural activities across multiple temporal scales. By applying MSE analysis on MEG signals, it is possible to capture information of intra-region neuronal interactions in millisecond resolution. Loss of complexity [35,62], towards both regularity and uncorrelated randomness, is regarded as the representation of pathologic dynamics [32,35–37,47,61,63], including Alzheimer's disease [42,43,47,64,65] and schizophrenia [43,58,61].

However, there remains a paucity of evidence on the spontaneous neural complexity at rest in chronic recurrent menstrual pain. Recently, we applied MSE estimation to MEG signals in PDMs in the presence of painful menstruation (state-related changes) for pain level prediction [26]. We found that MSE calculated from source activities could be used to predict pain scores, and the degree of hemispheric asymmetry in both source-level and sensor-level brain complexity reveals the intensity of pain.

Pain chronicity in PDM leads to functional neuroplasticity changes [13] and structural reorganization [18] (trait-related changes). In this study, we further extend our work with a large study cohort (156 participants) to examine whether PDMs' brain complexity in the absence of painful physiological state differs from those in healthy female controls (CONs). Complexity and spectral features of brain activity were extracted from resting-state MEG signals. MSE analysis revealed

significant alterations in brain complexity, whereas only limited alterations were detected through spectral analyses. The correlations between brain complexity features and clinical manifestations were also investigated. This paper is organized as follows: Section 2 elucidates the study sample, clinical and psychological assessments, brain signal acquisition and data analysis, and statistical analyses to investigate the group differences between PDMs and CONs. Section 3 presents our results. In Section 4 we discuss and compare our findings with previous studies.

2. Materials and Methods

2.1. Participants

In this study, we included a subset of the participants from our multimodal imaging studies of PDM in Taiwan [11]. Readers should refer to our recent studies [13,24] for detailed inclusion and exclusion criteria for PDMs and CONs. CONs had to meet all the same inclusion criteria, except that they must have no menstrual pain experience. All PDMs underwent pelvic ultrasonography to exclude organic pelvic diseases and were clinically diagnosed by a registered gynecologist. No analgesics were used within 24 h prior to the experiment [24].

Data from 82 PDMs and 79 age-matched CONs collected during pain-free periovulatory phase (Day 12–14 of menstruation) were included in our group analysis dataset. Due to the incompleteness of psychological inventory answers in a few participants, psychological data of 80 PDMs and 76 CONs were eventually included in our statistical analyses. This study was conducted in accordance with the Declaration of Helsinki. Written informed consent form and psychological inventories were approved by the ethics committee of Institutional Review Board of Taipei Veterans General Hospital, Taiwan. Before the study, all participants assessed for eligibility signed the written informed consent form.

2.2. Demographic, Menstrual Features, Pain Experiences, and Psychological Characteristics

Demographic data included age, body mass index (BMI), and handedness; menstrual features included age at menarche, years of menstruating, and averaged menstrual cycle length. Menstrual pain experiences were evaluated only in PDMs. Different aspects of recalled overall menstrual pain intensity over the last six months were evaluated in PDMs using McGill Pain Questionnaire (MPQ) [66,67] and verbal numerical rating scale (VNRS). MPQ total pain rating index (PRI-Total) composes four components: sensory, affective, evaluative, and miscellaneous; MPQ present pain index (PPI) is a 1-to-5 intensity scale (1 = mild, 5 = excruciating). VNRS was reported as menstrual pain recalled score with a range of 0 to 10 (0 = not at all, 10 = the worst imaginable pain).

Quality of life, personality traits, depressive mood, anxiety, and pain catastrophizing were assessed in all participants. The International Quality of Life Assessment Short-form-36 (IQOLA SF-36) Taiwan Standard Version 1.0 [68,69] (hereinafter, SF-36) was used to assess long-term physical and mental quality of life. The Chinese version of Basic Personality Inventory (BPI) [70] was used to assess personality traits, especially the personal emotional adjustment scale cluster (depression, anxiety, and hypochondriasis scales). Psychological inventories for anxiety and depression included Spielberger State-Trait Anxiety Inventory (STAI) [71], Beck Depression Inventory-IA (BDI-IA) [72], and Beck Anxiety Inventory (BAI) [73]. Pain Catastrophizing Scale (PCS) [74] was used to study the negative appraisal style of pain.

2.3. Data Acquisition

2.3.1. Resting-State Magnetoencephalography (MEG) Signals Acquisition

A whole-head 306-channel neuromagnetometer (Vectorview, Elekta Neuromag, Helsinki, Finland) comprising 102 triple sensors (two orthogonal planar gradiometers and one magnetometer) was used to record the resting-state MEG signals. Electrooculography (EOG) from two vertical (VEOG) and two horizontal (HEOG) electrodes were recorded. A 3D digitizer (Isotrak 3S10002, Polhemus, Colchester, VT, USA) was used to identify the initial locations of four head position indicator (HPI)

coils and three anatomical landmarks (nasion and bilateral preauricular points). The online sampling rate was 1000 Hz; online bandpass filter was 0.03–330 Hz; notch filter was 60 Hz. EOG signals exceeding 600 μV and MEG signals exceeding 6000 fT/cm were online-artifact rejected. MEG signals recorded from 102 gradiometers were excluded due to the susceptibility to distant noises, leaving signals from 204 planar gradiometers for further analyses.

Participants sat comfortably in a magnetically shielded room with their heads surrounded by the MEG helmet. Eye-closed resting-state MEG signals were recorded for three minutes in which the participants were instructed to relax, eliminate eye movements, and focus only on their breathing.

2.3.2. Structural MRI T1 Images Acquisition

T1-weighted brain images were acquired using a 3 Tesla magnetic resonance imaging (MRI) scanner (Magnetom Trio Tim, Siemens, Erlangen, Germany) with 12-channel head coil and standard three-dimensional magnetization-prepared rapid gradient-echo (3D MP-RAGE) sequence. The parameters were as follows: TR = 2530 ms, TE = 3.03 ms, TI = 1100 ms, flip angle = 7° , field-of-view (FOV) = $224 \times 256 \text{ mm}^2$, number of slices = 192, matrix size = 224×256 , thickness = 1 mm.

2.4. Source Analyses

2.4.1. Preprocessing

Eight-second epochs were extracted from the three-minute eye-closed recordings without temporal overlap to avoid potential temporal dependency and were eliminated if their amplitudes in any channel at any time point exceeded 2000 fT/cm. To prevent the MEG recordings from the interference of eye movement and eye blinks, epochs with an amplitude of any EOG channel exceeding 250 μV were also eliminated. This resulted in an average of 14 (standard deviation = 5) artifact-free eight-second epochs and 8000 data points per epoch (with a sampling rate of 1000 Hz). For each epoch, MEG signals were projected onto a signal subspace using the signal space projection method [75]. The projected signals were then passed through a 0.5–90 Hz band-pass filter followed by a 55–65 Hz band-stop filter for the elimination of power line interference. To remove the trend of the recordings, zero-mean adjustment was applied to signals of each channel.

2.4.2. Source Reconstruction

Maximum contrast beamformer [76] was used to estimate brain activity from MEG signals. To obtain the approximate source signal $y(t)$ of the dipole source θ , a spatial filter w_θ was applied to the MEG recordings $m(t)$:

$$y(t) = w_\theta^T m(t) \quad (1)$$

The spatial filter was obtained by applying the unit-gain constraint $w_\theta^T l_\theta = 1$ and minimizing variance of the signal $y(t)$:

$$\hat{w}_\theta = \underset{w_\theta}{\operatorname{argmin}} (E[\|y(t) - E[y(t)]\|^2] + \alpha \|w_\theta\|^2) \text{ subject to } w_\theta^T l_\theta = 1 \quad (2)$$

where $E[\cdot]$ denotes the expectation operator, l_θ denotes the lead field vector of the dipole source θ , and α is the Tikhonov regularization parameter [77], which can restrict the norm of w_θ . The estimated brain activity can be calculated by multiplying the MEG signals by the spatial filter \hat{w}_θ .

2.5. Feature Extraction

Three types of scale-invariant features were extracted from the estimated source activity, including brain complexity features (sample entropy, multiscale sample entropy, Shannon spectral entropy, Lempel-Ziv complexity), brain spectral features (relative band power, median frequency, spectral edge

frequency), and indices of hemispheric asymmetry (A). For each epoch and each subject, we calculated the features of each brain region using the following methods.

2.5.1. Feature Extraction of Brain Complexity Features via Nonlinear Analysis

Sample Entropy

Sample entropy (SE) proposed by a previous study [34] can be used to measure complexity. Two parameters, m and r , in SE refer to the length of the patterns to be compared ($m = 2$ in this study) and the tolerance range, respectively. Value r is usually set by $c \times \sigma$, where c is a constant ($c = 0.25$ in this study) and σ is the standard deviation of the signal. Given a signal containing N sample points, $x = [x_1, x_2, \dots, x_N]$. First, a vector of length m was defined by:

$$x_m(i) = [x_i, x_{i+1}, \dots, x_{i+m-1}], \text{ where } i = 1, \dots, N - m \quad (3)$$

Next, for $1 \leq j \leq N - m$ and $j \neq i$, the distance of two vectors $x_m(i)$ and $x_m(j)$ was calculated as the maximum value of the difference between corresponding elements, as follows:

$$\text{dist}(x_m(i), x_m(j)) = \max_{k=1,2,\dots,m} (\|x_{i+k-1} - x_{j+k-1}\|) \quad (4)$$

For each $i, i = 1, \dots, N - m$, if $\text{dist}(x_m(i), x_m(j)) \leq r$ then $x_m(i)$ and $x_m(j)$ were matched and the number of matching count, l_r^m , was increased by one. Then we defined vectors of length $m + 1$ by:

$$x_{m+1}(i) = [x_i, x_{i+1}, \dots, x_{i+m}], \text{ where } i = 1, \dots, N - m \quad (5)$$

and calculate the number of matching l_r^{m+1} . Once the l_r^m and l_r^{m+1} were obtained, the SE of the signal x can be obtained as follows:

$$\text{SE}(m, r, x) = -\ln \frac{l_r^{m+1}}{l_r^m} \quad (6)$$

Multiscale Sample Entropy

MSE can be used to further measure complexity over different time scales [36]. The coarse-grained time series $z^\tau = [z_1^\tau, z_2^\tau, \dots, z_{N/\tau}^\tau]$ of the original time series $x = [x_1, x_2, \dots, x_N]$ is obtained according to scale factor τ :

$$z_j^\tau = \frac{1}{\tau} \sum_{i=(j-1)\tau+1}^{j\tau} x_i, \quad 1 \leq j \leq \frac{N}{\tau} \quad (7)$$

We can obtain the multiscale SE of each time scale factor τ (τ is set from 1 to 100 in this study) by applying the SE method to each time series z_j^τ [26]. Given $m = 2$, $r = 0.25 \times \sigma$, $N = 1000 \text{ Hz} \times 8 \text{ s/epoch} = 8000$ data points per epoch, and $\tau = 1$ to 100, we had 80 to 8000 data points ($N/\tau = 8000/100$ to $8000/1$) for multiscale time-series data. The amount of data points was sufficient for SE calculation, as recommended in [34,78] (at least 10^m and preferable 30^m , that is, 100 to 900). Moreover, a minimum of 50 data points was also reported in EEG/MEG [52,79] and fMRI [28,60] studies. Figure 1 illustrates examples of time series data ranging from fine to coarse scales.

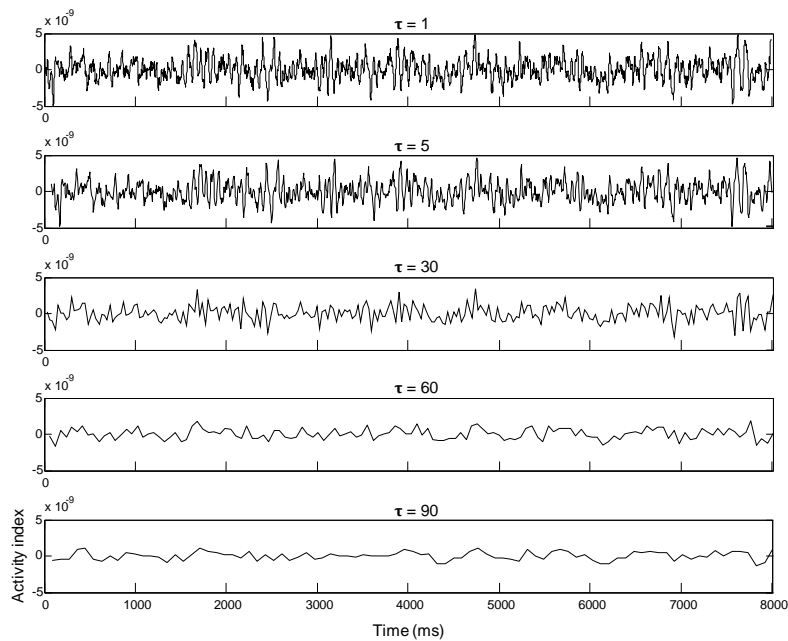


Figure 1. Examples of time series data for an 8-s epoch over a range of representative scale factors (τ) from fine to coarse scales: 1, 5, 30, 60 and 90. The x -axis represents time and the y -axis represents the estimated brain activity index.

Shannon Spectral Entropy

We applied Shannon entropy [80] to amplitude components of the normalized power spectrum density (PSD_n) as probability in Shannon entropy. Shannon spectral entropy (SSE) is a method to quantify the flatness of the PSD_n , which implies the irregularity of signal. The SSE is defined as the following equation:

$$SSE = - \sum_{f=0.5 \text{ Hz}}^{90 \text{ Hz}} PSD_n(f) \ln[PSD_n(f)] \quad (8)$$

where $PSD_n(f)$ is normalized PSD of the total power between 0.5 Hz and 90 Hz and is written by the following equation:

$$PSD_n(f) = \frac{PSD(f)}{\sum_{i=0.5 \text{ Hz}}^{90 \text{ Hz}} PSD(i)} \quad (9)$$

A high value of SSE means that the power spectral density is uniformly distributed whereas a low value of SSE means that the spectral concentrates at few frequencies. White noise has a high value of spectral entropy, whereas a signal composed of sinusoids has a low value of spectral entropy.

Lempel-Ziv Complexity

The analysis of Lempel-Ziv complexity (LZC) [81] is based on a finite symbol sequence, so the given signal must be coarse-grained by transforming it into a sequence with only a few symbols. Readers may consult Appendix A for the estimation and equations of LZC we used.

2.5.2. Feature Extraction of Brain Spectral Features in the Frequency Domain

Relative Band Power

In this study, the frequency band for analysis was set between 0.5 and 90 Hz and six frequency sub-bands were defined: δ (0.5–4 Hz), θ (4–8 Hz), α (8–12 Hz), β (12–30 Hz), $L\gamma$ (30–55 Hz),

and H γ (65–90 Hz). For each frequency sub-band (B), we calculated the relative band power (RP(B)) as the ratio of the overall power in that frequency sub-band to that of the entire frequency band:

$$RP(B) = \frac{\sum_{f \in B} PSD(f)}{\sum_{f=0.5 \text{ Hz}}^{90 \text{ Hz}} PSD(f)} \quad (10)$$

where PSD(f) is the power spectrum density of frequency f .

Median Frequency

Median frequency (MF) is a measure which summarizes the information of the entire power spectrum [56] and can be defined as the frequency which accounts for 50% of the total power. MF can be regarded as a rough representation of the distribution of power spectrum. It is written by the following equation:

$$0.5 \sum_{f=0.5 \text{ Hz}}^{90 \text{ Hz}} PSD(f) = \sum_{f=0.5 \text{ Hz}}^{\text{MF}} PSD(f) \quad (11)$$

Spectral Edge Frequency

Just like median frequency, spectral edge frequency 90 (SEF90) is defined as the frequency which accounts for 90% of the total power. SEF90 has been applied to study the depth of anesthesia [82] and Alzheimer's disease [64], and it is written as the following equation:

$$0.9 \sum_{f=0.5 \text{ Hz}}^{90 \text{ Hz}} PSD(f) = \sum_{f=0.5 \text{ Hz}}^{\text{SEF90}} PSD(f) \quad (12)$$

2.5.3. Regional Features of Resting-State Networks

Brain complexity and spectral features were calculated from the estimated source activity at each voxel and were averaged across all eight-second epochs. For cortical-level analysis, 90 brain regions (45 regions in each hemisphere) were defined using an automated anatomical labeling (AAL) template [83] with a 1 mm \times 1 mm \times 1 mm resolution, which is available in the MRIcro medical image viewer freeware [84]. The AAL label of each voxel was obtained by registering the AAL template to each participant's MRI T1 anatomical images using IBASPM (Individual Brain Atlases using Statistical Parametric Mapping) [85], an extension of the image analysis academic software toolkit Statistical Parametric Mapping version 5 (SPM5). To be noted, AAL region whose averaged voxel number across all participants was less than 10 voxels (that is, volume smaller than 10 mm³) were excluded from further statistical analysis. Subsequently, brain features were averaged across all voxels within each region, yielding one representative mean value for each brain feature at each brain region.

To characterize resting-state functional brain activities, the brain regions were categorized into eight resting-state networks (RSNs) based on literature review: limbic network (LIMBIC) [86–88], default mode network (DMN) [86,89–101], salience network (SAN) [92,93,102], sensorimotor network (SMN) [86,92,93,97,103], executive control network (ECN) [86,92,93,97,102,104,105], attention network (AN; including dorsal and ventral attention network; DAN and VAN) [86,92–94,97,106,107], visual processing network (VIS) [86,92,97,108], and auditory processing network (AUD) [86,92,97]. Brain regions and corresponding RSNs are listed in Supplementary Materials Table S1, where each region might be indicated in at most four RSNs because the same region might engage in different RSNs simultaneously [109]. Same RSN categories were assigned to the same brain region in the left and right hemispheres.

2.5.4. Asymmetry Features

Subsequently, the indices of hemispheric asymmetry (A) for each region were calculated by using:

$$A = \frac{R - L}{R + L} \quad (13)$$

where R and L denote one of the features in the corresponding brain regions in the right and left hemispheres, respectively. The more positive the A was, the larger the MSE value in the right hemisphere compared to that in the left hemisphere for that feature; the more negative the A was, the larger the MSE value in the left hemisphere compared to that in the right hemisphere for that feature.

2.6. Statistical Analyses

2.6.1. Demographic, Menstrual Features, Pain Experiences, and Psychological Characteristics

Demographic data, menstrual features, menstrual pain experiences, and psychological scores of PDMs and CONs were processed in IBM SPSS Statistics 22.0 software (IBM Corp., Armonk, NY, USA). Prior to any inferential statistical testing, descriptive statistical tests and normality tests (Shapiro-Wilk test) [110] were performed in each group. Since some of the psychological data were not normally distributed, Mann-Whitney U tests ($\alpha = 0.01$, two-tailed) were subsequently applied to compare group differences. Median, interquartile range (IQR, 25% to 75%), p values, and Mann-Whitney U scores were reported accordingly.

2.6.2. Brain Features

To investigate the effect of long-term menstrual pain on brain complexity, spectral, and hemispheric asymmetry features, permutation testing based upon t -statistics [111] were performed to deal with the multiple comparisons problem. In permutation tests, all participants were randomly divided into two groups with the same size as the original data set (80 PDMs vs. 76 CONs). This procedure was repeated 5000 times (5000 permutations) for each brain region and for each feature to compare group differences. Each time a new t -test compared two randomly divided “groups” and gave one t -score. As a result, a distribution of 5000 t -scores was created. Only p -values within the 5% of the lower or higher values ($\alpha = 0.05$) were considered statistically significant for complexity and spectral features, or 1% ($\alpha = 0.01$) for asymmetry features. To further examine whether there is global or network-wise effect of long-term menstrual pain on MSE, we performed the following four independent t -tests (two-tailed, $\alpha = 0.05$) by comparing the averaged MSE values in two-groups across (i) the whole brain for each scale factor; (ii) each network for each scale factor; (iii) each network in each hemisphere for each scale factor, and (iv) all scale factors in each brain region. In addition, to delineate significant hemispheric asymmetry (lateralization) in each group, for each significant between-group hemispheric asymmetry feature, we further examined significant within-group hemispheric asymmetry by comparing the mean value of that feature in the left versus right hemispheres in each group using Wilcoxon sign-rank tests ($\alpha = 0.05$, two-tailed) (as reported in Supplementary Materials Tables S2–S4). BrainNet viewer visualization tool [112] was used to depict the significant differences.

2.6.3. Correlations between Pain Experiences, Psychological Traits, and Brain Features

To understand how clinical and psychological levels of long-term menstrual pain correlate with the altered brain complexity and spectral features (physiological level), we analyzed how PDMs’ menstrual pain experiences, anxiety, depression, and pain catastrophizing characteristics were correlated with brain features that differed significantly between PDMs and CONs. Spearman correlations ($\alpha = 0.01$, two-tailed) were carried out in IBM SPSS Statistics 22.0 software.

3. Results

3.1. Demographic, Menstrual Features, Pain Experiences, and Psychological Characteristics

3.1.1. PDMs and CONs had Similar Demographic Characteristics and Menstrual Features

Table 1 shows the demographic characteristics and menstrual features from 80 PDMs and 76 CONs. As expected, PDMs and CONs had similar demographic characteristics and menstrual features, indicating that PDMs in this study were otherwise-healthy females. Hence, any group differences found in further analyses were not likely to be contributed by demographic and menstrual features.

3.1.2. PDMs Experienced Long-Term Moderate-to-Severe Menstrual Pain

Table 1 also shows the clinical manifestations of menstrual pain experiences in 80 PDMs. PDMs in our study have been suffering from moderate-to-severe menstrual pain (7 in the 0–10 scale; IQR: 6–8) lasting for two days (IQR: 1–3) every month for about eight years (IQR: 6–10). The recalled present pain index (McGill Pain Questionnaire PPI) of menstrual pain over the last six months also showed that PDMs experienced moderate-to-severe menstrual pain (3 in the 1–5 scale; IQR: 2–4).

Table 1. Demographic characteristics, menstrual features, and clinical manifestations of menstrual pain experiences. PDMs and CONs had similar demographic characteristics and menstrual features.

Demographic and Clinical Manifestations	PDM (<i>n</i> = 80)	CON (<i>n</i> = 76)	Between-Group (<i>p</i>)	Mann-Whitney U
Demographic characteristics				
Age (y/o)	22.78 (22–25)	23.87 (22–26)	0.036	2449.5
BMI	20.11 (19–22)	20.55 (19–23)	0.560	2142.5
Edinburgh handedness (%)	86.67 (70–100)	89.00 (70–100)	0.723	2867.5
Menstrual features				
Age at menarche (y/o)	12 (11–13)	12 (12–13)	0.131	2591.0
Years of menstruating (y)	10 (9–12)	11 (10–13)	0.248	2679.5
Menstrual cycle length (d)	30 (28–30)	30 (29–30)	0.627	2796.5
Menstrual pain experiences				
Age of PDM onset (y/o)	14.5 (13–16)	-	-	-
Menstrual pain history (y)	8 (6–10)	-	-	-
Menstrual pain duration (d)	2 (1–3)	-	-	-
Absenteeism (%)	54.7	-	-	-
Medication (%)	54.8	-	-	-
Menstrual pain recalled score (0–10)	7 (6–8)	-	-	-
MPQ: Recalled PPI (1–5)	3 (2–4)	-	-	-
MPQ: Recalled PRI—Total (0–78)	36 (28–45)	-	-	-
Sensory (0–42)	18 (13–24)	-	-	-
Affective (0–14)	4 (2–9)	-	-	-
Evaluative (0–5)	4.5 (1–5)	-	-	-
Miscellaneous (0–17)	9 (6–12)	-	-	-

Group differences were compared using Mann-Whitney U test ($p < 0.01$, two-tailed). Unit or range is bracketed after each item name. Data are presented as median (IQR). Menstrual pain recalled score, recalled PPI, and recalled PRI scores are average recalled menstrual pain intensities over the last six months. PDM, primary dysmenorrhea patients; CON, healthy female controls; BMI, body mass index; MPQ, McGill pain questionnaire; PRI, pain rating index; PPI, present pain index; y/o, years old; y, year, d, day.

3.1.3. PDMs Displayed Significantly Higher Anxiety, Depression, and Pain Catastrophizing Characteristics than CONs

Table 2 displays the results of quality of life, personality traits, anxiety, depression, and pain catastrophizing characteristics in both PDMs and CONs. After long-term menstrual pain, PDMs manifested significantly lower quality of life in both physical well-being ($p < 0.00001$) and mental well-being ($p < 0.00001$). Group differences regarding the psychological traits and mental health conditions were more alarming: compared to CONs, PDMs exhibited higher personal emotional adjustment problems (anxiety, $p = 0.00068$; depression, $p = 0.00003$; hypochondriasis, $p < 0.00001$),

anxiety (BAI, $p = 0.00014$; state anxiety, $p = 0.00007$; trait anxiety, $p < 0.00001$), pain catastrophizing characteristics (helplessness, $p < 0.00001$; magnification, $p < 0.00001$; rumination, $p < 0.00001$), and marginal significantly higher of depressive mood ($p = 0.01307$).

Table 2. Between-group comparison of psychological assessments. PDMs displayed significantly lower quality of life and higher anxiety, depression, and pain catastrophizing characteristics than those of CONs.

Psychological Assessment	PDM ($n = 80$)	CON ($n = 76$)	Between-Group (p)	Mann-Whitney U
Quality of life				
SF-36 total scores (0–200)	96.25 (83–104)	111.35 (106–115)	<0.00001 [†]	960.00
PCS (Physical; 0–100)	50.14 (43–54)	55.00 (52–58)	<0.00001 [†]	1387.0
MCS (Mental; 0–100)	46.88 (41–54)	56.66 (50–61)	<0.00001 [†]	1617.5
Personality traits				
BPI: Personal emotional adjustment scale cluster				
Anxiety (0–14)	5 (3–8)	4 (2–6)	0.00068 [*]	2055.5
Depression (0–14)	2.5 (1–6)	1 (0–2)	0.00003 [*]	1844.5
Hypochondriasis (0–14)	5 (3–7)	2 (1–3)	<0.00001 [†]	1420.5
Depressive mood				
BDI (0–63)	4 (1–11)	3 (1–6)	0.01307	2344.0
Anxiety				
BAI (0–63)	5 (2–10)	2 (1–5)	0.00014 [*]	1969.5
STAI total scores (40–160)	83 (71–91)	70 (62–77)	<0.00001 [†]	1471.0
State anxiety (20–80)	37 (33–42)	32 (28–36)	0.00007 [*]	1888.0
Trait anxiety (20–80)	45 (38–50)	37 (32–41)	<0.00001 [†]	1403.5
Pain catastrophizing				
PCS total score (0–52)	17 (9–24)	3 (0–8)	<0.00001 [†]	1121.0
Pain helplessness (0–16)	7 (4–12)	1 (0–4)	<0.00001 [†]	1172.0
Pain magnification (0–24)	3 (1–4)	1 (0–2)	<0.00001 [†]	1595.0
Pain rumination (0–12)	7 (3–10)	1 (0–3)	<0.00001 [†]	1116.0

Significant between-group differences were tested using Mann-Whitney U tests ($p < 0.01$, two-tailed). ^{*} $p < 0.001$, [†] $p < 0.00001$. Unit or range is bracketed after each item name. Data are presented as median (IQR) with IQR displayed as integers due to space limitation. PDM, primary dysmenorrhea patients; CON, healthy female controls; SF-36, International Quality of Life Assessment Short-form-36 Taiwan standard version 1.0; PCS, physical component summary; MCS, mental component summary; BPI, basic personality inventory; BDI, Beck depression inventory; STAI, Spielberger state-trait anxiety inventory; BAI, Beck anxiety inventory; PCS, pain catastrophizing scale.

3.2. Brain Complexity, Spectral, and Hemispheric Asymmetry Features

3.2.1. Brain Complexity Feature: Multiscale Sample Entropy

Figure 2 shows the group differences between PDMs and CONs in brain complexity featured by MSE, and are quite revealing in several ways. First, significant group differences only emerged at larger scale factors (SFs) beginning from SF 52 (Figure 2a,b). Second, counts of significant group differences within each scale factor-interval were SFs 1~50 (0), 51~60 (4), 61~70 (8), 71~80 (6), 81~90 (10), and 91~100 (14). SF 92 was the most frequent feature (count = 4) that differentiated the brain complexity of PDMs from CONs, followed by SF 81 and SF 99 (3 counts each) (Figure 2a). Third, what stands out from the bird's-eye view in Figure 2c is that MSE values in PDMs were mostly lower (blue spheres) than those in CONs, and the differences emerged mainly in the right hemisphere. Table 3 reveals that compared to CONs, PDMs showed decreased MSE in chronic pain-related brain regions such as limbic/subcortical regions (amygdala, hippocampus, parahippocampal gyrus), default mode network (angular gyrus, inferior parietal lobule, precuneus, inferior temporal gyrus, middle temporal gyrus), and pain sensory-related regions such as sensorimotor network (rolandic operculum, thalamus), indicating a loss of complexity in chronic pain-related regions after long-term menstrual pain. Conversely, PDMs demonstrated higher MSE values than did CONs at the anterior cingulate cortex (ACC), the key region in salience network and also an important pain-regulating region. No significant group differences in all global or network-wise tests were found.

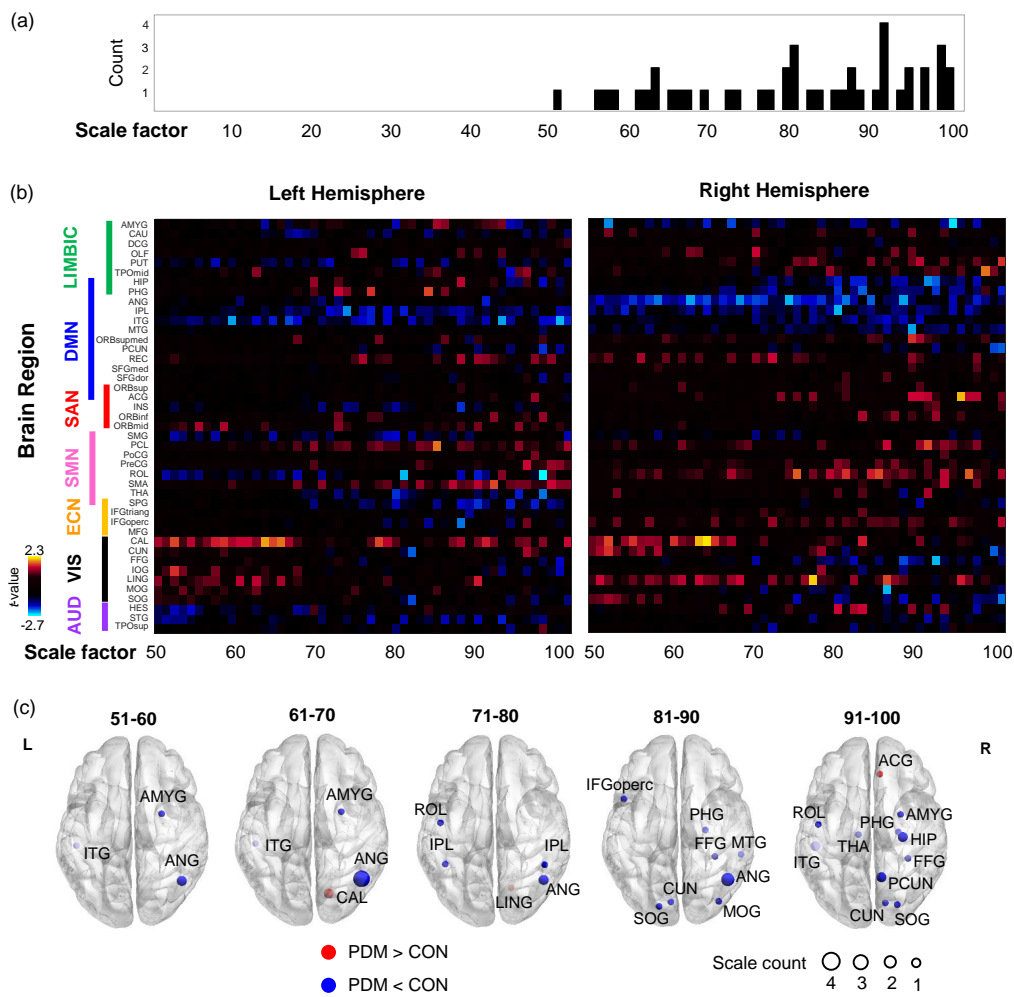


Figure 2. Significant multiscale sample entropy (MSE) group differences from resting-state MEG brain signals during pain-free state. MSE values of PDMs were mostly lower than those of CONs. Significant MSE group differences were found at larger scale factors (SFs) and mainly in the right hemisphere. (a) Histogram of the number of regions showing significant group differences (permutation testing with 5000 iterations, $p < 0.05$, two-tailed) from SFs 1 to 10: SFs 1~50 (0), 51~60 (4), 61~70 (8), 71~80 (6), 81~90 (10), and 91~100 (14). Top three: SF 92 (count = 4), SF 81 (count = 3), and SF 99 (count = 3); (b) MSE group differences. The x-axis represents the SFs of MSE ranging from 51 to 100. The y-axis represents the AAL brain regions, which were categorized into different RSNs (indicated by thick lines and text in different colors) for functional attribution. The color bar represents between-group t -values after 5000 permutation tests, with the most positive t -values (PDMs > CONs) shown in bright yellow and the most negative t -values (PDMs < CONs) shown in bright blue; (c) Brain regions that revealed significant MSE group differences were grouped into five SF-intervals for demonstration: SFs 51~60, 61~70, 71~80, 81~90 and 91~100. Brain regions where MSE measures in PDMs were higher or lower than those in CONs are represented in red or blue spheres, respectively. Size of sphere represents the count of scale factors that showed significant group differences. PDM, primary dysmenorrhoea patients; CON, healthy female controls; L, left hemisphere; R, right hemisphere; LIMBIC, limbic network; DMN, default mode network; SAN, salience network; SMN, sensorimotor network; ECN, executive control network; AMYG, amygdala; ANG, angular gyrus; ITG, inferior temporal gyrus; CAL, calcarine; ROL, rolandic operculum; IPL, inferior parietal lobule; LING, lingual gyrus; IFGoperc, opercularis of inferior frontal gyrus; SOG, superior occipital gyrus; CUN, cuneus; PHG, parahippocampal gyrus; FFG, fusiform gyrus; MTG, middle temporal gyrus; MOG, middle occipital gyrus; ACG, anterior cingulate gyrus; THA, thalamus; HIP, hippocampus; PCUN, precuneus.

Table 3. Significant group differences in multiscale sample entropy ($p < 0.05$, 5000 permutation tests).

Contrast/RSN	Brain Region	L/R	Abbr.	Count	Scale Factor	<i>t</i> Score (Range)	<i>p</i> Value (Range)	
PDM < CON								
LIMBIC	Amygdala	R	AMYG.R	3	52, 67, 94	−2.601~−2.058	0.0110~0.0400	
	Hippocampus	R	HIP.R	2	91~92	−2.238, −2.136	0.0244, 0.0364	
	Parahippocampal g.	R	PHG.R	2	83, 92	−2.085, 1.985	0.0392, 0.0450	
DMN	Angular g.	R	ANG.R	11	57~58, 62, 64, 68, 70, 74, 78, 81, 84, 88	−2.418~−1.988	0.0146~0.0462	
		L	IPL.L	1	73	−2.283	0.0252	
		IPL	R	IPL.R	1	80	−2.406	0.0196
	Precuneus	R	PCUN.R	2	99~100	−2.124~−2.034	0.0338, 0.0430	
	ITG	L	ITG.L	4	59, 66, 92, 99	−2.368~−2.031	0.0162~0.0424	
	MTG	R	MTG.R	1	89	−2.331	0.0220	
	SMN	Rolandic operculum	L	ROL.L	2	80, 97	−2.690~−2.406	0.0044~0.0172
	Thalamus	L	THA.L	1	97	−2.222	0.0274	
ECN/VAN	IFG, opercular	L	IFGoperc.L	1	87	−2.175	0.0278	
VIS	Cuneus	L	CUN.L	1	81	−2.118	0.0322	
		R	CUN.R	1	99	−2.087	0.0368	
	Fusiform g.	R	FFG.R	2	88, 92	−2.452, −2.017	0.0140, 0.0412	
	MOG	R	MOG.R	1	86	−2.407	0.0178	
	SOG	L	SOG.L	1	81	−2.024	0.0424	
		R	SOG.R	1	100	−2.186	0.0314	
PDM > CON								
SAN	ACC	R	ACG.R	1	95	2.061	0.0404	
VIS	Calcarine	R	CAL.R	2	63~64	2.015~2.188	0.0256~0.0446	
	Lingual g.	R	LING.R	1	77	2.111	0.0350	

PDM, primary dysmenorrhea patients; CON, healthy female controls; RSN, resting-state network; L, left hemisphere; R, right hemisphere; g., gyrus; DMN, default mode network; SMN, sensorimotor network; ECN, executive control network; VIS, visual processing network; SAN, salience network; g.: gyrus; IPL, inferior parietal lobule; ITG, inferior temporal gyrus; MTG, middle temporal gyrus; IFG, inferior frontal gyrus; MOG, middle occipital gyrus; SOG, superior occipital gyrus; ACG, anterior cingulate gyrus.

3.2.2. Hemispheric Asymmetry of Multiscale Sample Entropy

Table 4 summarizes the significant group differences of hemispheric asymmetry of MSE (asymMSE). We summed their counts within each SF-interval: SFs 1~10 (1), 11~20 (2), 21~30 (7), 31~40 (13), 41~50 (13), 51~60 (11), 61~70 (4), 71~80 (4), 81~90 (5), and 91~100 (4). Unlike MSE, which group differences only emerged at larger scale factors (SFs), asymMSE group differences were distributed across all SF-intervals with the most seen between SFs 31~60 (Figure 3a).

Table S2 displays the lateralization of MSE within PDM and CON groups sorted by scale factor intervals and hemispheric asymmetry alteration in PDMs, as depicted in Figure 3c. We found that CON group exhibited mostly left-lateralization. In contrast, as presented in Table S3, PDMs exhibited altered hemispheric asymmetry, including loss of asymmetry across different scales (count = 48), enhanced left-lateralization at the limbic regions (count = 5), and enhanced right-lateralization at the default mode network regions (count = 8). Hemispheric asymmetry of brain complexity further exposed group differences that were not seen in MSE analysis, including those in the superior frontal gyrus (ORBsupmed, SFGdor, and SFGmed), orbital middle frontal gyrus (ORBmid), putamen, caudate, and Heschl's gyrus. The altered hemispheric asymmetry in PDMs may imply the changes of neurophysiological complexity associated with menstrual pain.

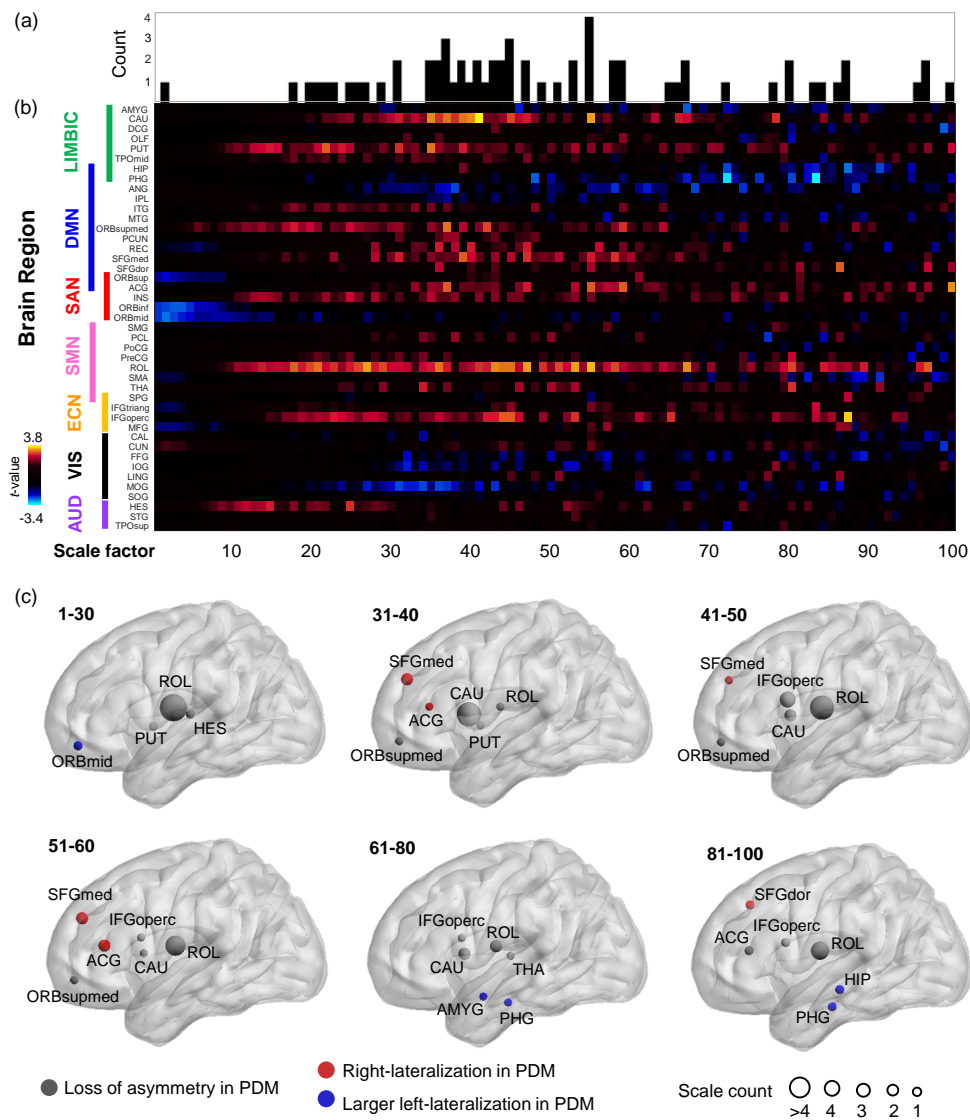


Figure 3. Hemispheric asymmetry of multiscale sample entropy (asymMSE) group differences from resting-state MEG brain signals during pain-free state. Significant group differences were found across all scale factor-intervals with the most differences seen between SFs 31~60. (a) Count of each SF that showed significant group differences (permutation testing with 5000 iterations, $p < 0.01$, two-tailed); (b) Group differences in hemispheric asymmetry of MSE (asymMSE). The *x*-axis represents the scale factors (SFs) of asymMSE ranging from 1 to 100; the *y*-axis represents the AAL brain regions which were categorized into different RSNs (indicated by thick lines and text in different colors) for functional attribution; the color bar represents between-group *t*-values after 5000 permutation tests ($\alpha = 0.01$) as listed in Table S2, with the most positive *t*-values (PDMs > CONs) shown in bright yellow and the most negative *t*-values (PDMs < CONs) shown in bright blue; (c) Altered hemispheric asymmetry of MSE in PDMs. Brain regions that revealed significant asymMSE group differences were grouped into six SF-intervals for demonstration (Table S2): SFs 1~30, 31~40, 41~50, 51~60, 61~80 and 81~100. CON group exhibited mostly left-lateralization. Compared to CONs, grey, red, and blue spheres indicate the brain regions with loss of hemispheric asymmetry, right-lateralization, and left-lateralization in PDMs, respectively. Size of sphere represents count of scale factors that showed significant group differences. PDM, primary dysmenorrhea patients; CON, healthy female controls; LIMBIC, limbic network; DMN, default mode network; SAN, salience network; SMN, sensorimotor network; ECN, executive control network; L, left hemisphere; R, right hemisphere; MFG, middle frontal gyrus; ORBmid, orbital MFG; ROL, rolandic operculum; PUT, putamen; HES, Heschl gyrus; SFG, superior frontal gyrus; ORBsupmed, medial orbital SFG; SFGmed, medial SFG; ACC, anterior cingulate gyrus; CAU, caudate; IFGoperc, opercularis of inferior frontal gyrus; AMYG, amygdala; PHG, parahippocampal g.; SFGdor, dorsolateral SFG; HIP, hippocampus; THA, thalamus.

Table 4. Significant group differences in hemispheric asymmetry of multiscale sample entropy ($p < 0.01$, 5000 permutation tests).

Contrast/ RSN	Brain Region	Abbr.	Count	Scale Factor	<i>t</i> Score (Range)	<i>p</i> Value (Range)
LIMBIC	Parahippocampal g.	PHG	2	72, 83	−3.393, −3.201	0.0012, 0.0016
	Amygdala	AMYG	1	67	−2.518	0.0080
	Hippocampus	HIP	1	87	−2.693	0.0092
	Caudate	CAU	11	35~41, 45, 55, 66, 78	2.613~3.752	0.0004~0.0096
	Putamen	PUT	3	22, 31, 35	2.663~3.020	0.0034~0.0080
DMN	SFG, medial orbital	ORBsupmed	3	37, 42, 59	2.660~3.050	0.0016~0.0088
	SFG, dorsolateral	SFGdor	2	86, 97	2.512, 2.958	0.0026, 0.0090
	SFG, medial	SFGmed	5	31, 39, 47, 55, 58	2.544~2.918	0.0056~0.0098
SAN	ACC	ACG	4	37, 55, 59, 100	2.876~3.139	0.0012~0.0050
	MFG, orbital	ORBmid	1	2	−2.671	0.0076
SMN	Rolandic operculum	ROL	23	18, 20~21, 23, 26~27, 29, 36, 41, 43~45, 47, 49, 51, 53, 55, 58, 67, 80, 84, 96~97	2.589~3.390	0.0006~0.0086
	Thalamus	THA	1	80	2.722	0.0072
ECN/VAN	IFG, opercular	IFGoperc	6	43~45, 53, 65, 87	2.608~3.474	0.0010~0.0094
AUD	Heschl g.	HES	1	25	2.695	0.0068

PDM, primary dysmenorrhea patients; CON, healthy female controls; g.: gyrus; RSN, resting-state network; LIMBIC, limbic network; DMN, default mode network; SAN, salience network; SMN, sensorimotor network; ECN, executive control network; AUD, auditory network; SFG, superior frontal gyrus; ACC, anterior cingulate gyrus; MFG, middle frontal gyrus; IFG, inferior frontal gyrus.

3.2.3. Brain Spectral Features, Other Complexity Features, and Their Hemispheric Asymmetry

No significant group differences were found in relative band power, median frequency, spectral edge frequency, Shannon spectral entropy, and Lempel-Ziv complexity. Significant group differences were only disclosed in the hemispheric asymmetry (asymSpectral) of high gamma relative band power, median frequency, and spectral edge frequency. PDMs showed left-lateralized asymSpectral mainly in the frontal regions, including ORBmid and ORBinf, and lingual gyrus, as seen in Figure 4 and Table 5. Overall, results from brain temporal and spectral features indicated that MSE might be more sensitive than spectral analyses in extracting spontaneous neurophysiological complexity of long-term menstrual pain over multiple time series.

Table 5. Significant group differences in asymmetry of spectral and other complexity features ($p < 0.01$, 5000 permutation tests).

Feature/Contrast	Brain Region	Abbr.	Count	<i>t</i> Score (Range)	<i>p</i> Value (Range)
Hemispheric asymmetry					
High gamma					
PDM < CON	IFG, orbital	ORBinf	1	−3.258	0.0014
PDM < CON	MFG, orbital	ORBmid	1	−2.600	0.0094
Median frequency					
PDM < CON	Lingual g.	LING	1	−3.463	0.0004
Spectral edge frequency					
PDM < CON	IFG, orbital	ORBinf	1	−3.130	0.0016

PDM, primary dysmenorrhea patients; CON, healthy female controls; L, left hemisphere; R, right hemisphere; g., gyrus; IFG, inferior frontal gyrus; MFG, middle frontal gyrus.

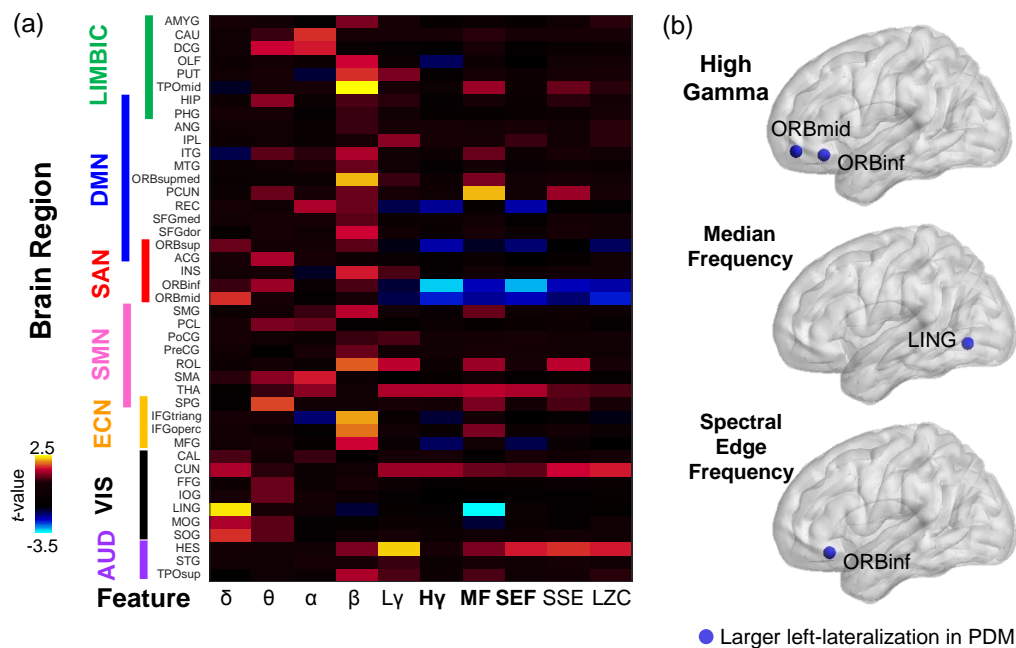


Figure 4. Group differences of hemispheric asymmetry of spectral and other complexity features from resting-state MEG brain signals during pain-free state. Significant group differences were only disclosed in hemispheric asymmetry of high gamma relative band power, median frequency, and spectral edge frequency, and were left-lateralized mainly in the frontal regions in PDMs. (a) Group differences in hemispheric asymmetry. The x -axis of the matrix represents the hemispheric asymmetry of spectral and other brain complexity features; the y -axis represents the AAL brain regions which were categorized into different RSNs (indicated by thick lines and text in different colors) for functional attribution; the color bar represents between-group t -values after 5000 permutation tests ($\alpha = 0.01$), with the most positive t -values (PDMs > CONs) shown in bright yellow and the most negative t -values (PDMs < CONs) shown in bright blue; (b) Hemispheric asymmetry alterations in PDMs were displayed (Table S4). Blue spheres depict the brain regions with enhanced left lateralization in PDMs compared to CONs. PDM, primary dysmenorrhea patients; CON, healthy female controls; L, left hemisphere; R, right hemisphere; g., gyrus; IFG, inferior frontal gyrus; MFG, middle frontal gyrus; ORBmid, orbital MFG; ORBinf, orbital IFG, orbital; LING, lingual gyrus; RP, relative band power; δ , RP(δ); θ , RP(θ); α , RP(α); β , RP(β); $L\gamma$, RP(*low* γ); $H\gamma$, RP(*high* γ); MF, median frequency; SEF, Spectral edge frequency; SSE, Shannon sample entropy; LZC, Lempel-Ziv complexity.

3.3. Correlations between Multiscale Sample Entropy and Pain Experiences/Psychological Characteristics

Table 6 presents the relationships between significant findings in MSE and PDMs' clinical pain experiences as well as their psychological characteristics. Spearman correlation analysis revealed that the higher the depression scores, the higher the brain complexity in the hippocampus ($\rho = 0.303$, $p = 0.0064$; Figure 5a), thalamus (BPI-Depression: $\rho = 0.329$, $p = 0.0029$; BDI: $\rho = 0.318$, $p = 0.0041$; Figure 5b), and angular gyrus (BDI: $\rho = 0.304$, $p = 0.0060$; scale factor 88: $\rho = 0.291$, $p = 0.0087$). Brain complexity in the Rolandic operculum was negatively correlated with physical well-being ($\rho = -0.296$, $p = 0.0085$; Figure 5c), and its asymmetry index was negatively correlated with depression score ($\rho = -0.304$, $p = 0.0061$). Brain complexity in the fusiform gyrus was positively correlated with pain magnification catastrophizing thought ($\rho = 0.300$, $p = 0.0072$). Brain complexity in the left inferior temporal gyrus was positively correlated with pain recalled score ($\rho = 0.323$, $p = 0.0045$). Interestingly, these relationships appeared primarily at larger (coarse) scale factors, suggesting that brain complexity at larger scale factors might reflect macroscopic changes at the psychological and/or behavioral levels.

Table 6. Correlations between multiscale sample entropy/hemispheric asymmetry of multiscale sample entropy and anxiety-, depressive-, and pain-related psychological characteristics in PDMs. ($p < 0.01$, two-tailed).

Feature	Brain Region	RSN	Psychological Score	Scale Factor	Rho	p Value
MSE	Hippocampus (R)	LIMBIC	BDI	91	0.303	0.0064
	Thalamus (L)	SMN/DMN/LIMBIC	BPI-Depression	97	0.329	0.0029
			BDI	97	0.318	0.0041
	ITG (L)	DMN	Pain recalled score	95	0.323	0.0045
	Rolandic operculum (L)	SMN	SF-36, Physical component	97	-0.296	0.0085
	Angular g. (R)	DMN/ECN/AN	BDI	84	0.304	0.0060
			BDI	88	0.291	0.0087
asymMSE	Fusiform g. (R)	VIS	PCS-Magnification	88	0.300	0.0072
	Parahippocampal g.	DMN/LIMBIC	BAI	72	0.348	0.0016
	Rolandic operculum	SMN	BPI-Depression	84	-0.304	0.0061
	SFG, medial	DMN	BPI-Depression	55	-0.321	0.0037

PDMs, primary dysmenorrhea patients; RSN, resting-state network; MSE, multiscale sample entropy; asymMSE, hemispheric asymmetry of MSE; SMN, sensorimotor network; DMN, default mode network; LIMBIC, limbic network; ECN, executive control network; AN, attention network; SAN, salience network; VIS, visual network; BPI, basic personality inventory; BDI, Beck depression inventory; PCS, pain catastrophizing scale; SF-36, International Quality of Life Assessment Short-form-36 Taiwan standard version 1.0; BAI, Beck anxiety inventory.

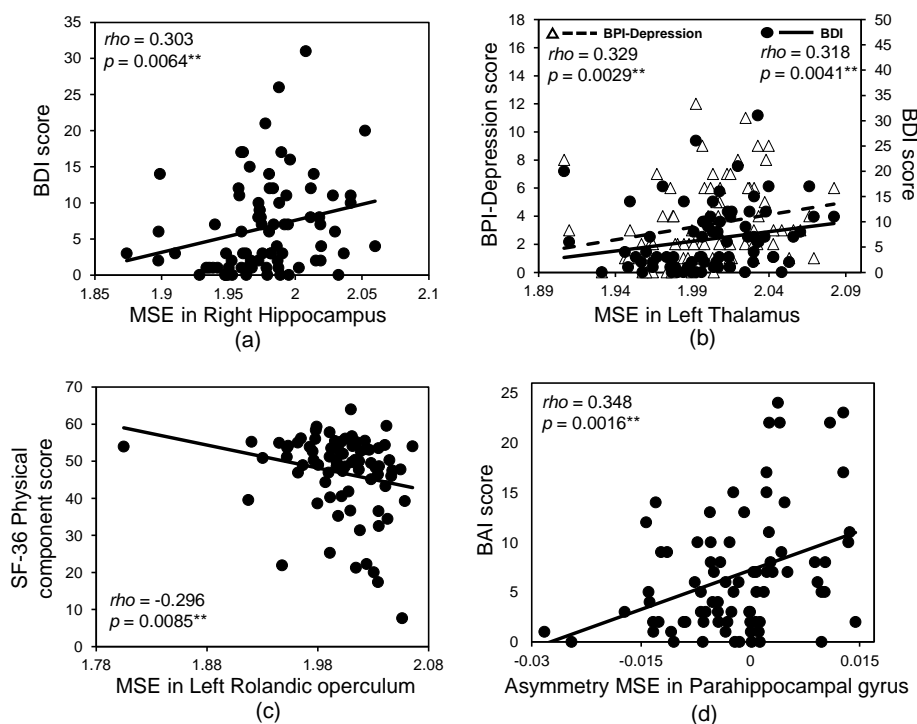


Figure 5. Spearman correlation between multiscale sample entropy and pain experiences or psychological characteristics in primary dysmenorrhea patients (PDMs). The x -axis of each subfigure is the value of MSE or hemispheric asymmetry of MSE (asymMSE) in each PDMs; the y -axis is the pain and/or psychological scores. Spearman ρ and p -values are listed for each correlation. (a) Brain complexity in the right hippocampus positively correlated with depression score; (b) Brain complexity in the left thalamus positively correlated with depression scores; (c) Brain complexity in the left Rolandic operculum negatively correlated with physical component score of quality of life; (d) Asymmetry of brain complexity in the parahippocampal gyrus was positively correlated with anxiety score. MSE, multiscale sample entropy; asymMSE, hemispheric asymmetry of MSE; BDI, Beck depression inventory; BAI, Beck anxiety inventory; PCS, pain catastrophizing scale; MPQ, McGill pain questionnaire; PRI, MPQ pain rating index; PPI, MPQ present pain index.

4. Discussion

In this study, we investigated the resting-MEG signals during pain-free state after long-term menstrual pain in a large study cohort (156 participants). The major finding of this study is that PDMs presented loss of complexity in brain regions associated with sensory, affective, and evaluative components of pain, including the thalamus, hippocampus, and anterior cingulate gyrus, even in the absence of menstrual pain. Our results demonstrated that MSE analysis serves as a good probe for changes of brain complexity sculptured by long-term pain experience.

4.1. Measures of Neural Complexity

PDMs experienced mental health consequences, including anxiety, depression, and pain catastrophizing characteristics. Our results are consistent with previous studies in depression, anxiety disorders, autistic spectrum disorder, bipolar disorder, and schizophrenia [35,42,61,64,113] that support the loss of complexity theory. Hornero et al. [47] reported that patients with Alzheimer's disease, characterized by degeneration of the nervous system that decreases regional dynamical complexity, exhibited less complex and more regular neural activities at rest. Similar "slowing effect" in Alzheimer's patients, that is, an increase of regularity of the signal and a reduction in complexity, was observed by Labate et al. [114,115] using entropic complexity measures. On the other hand, Brookes et al. [58] demonstrated that patients with schizophrenia, characterized by loss/breakdown of local synchrony (more disordered and increased randomness) and dysconnectivity between distributed brain regions, manifested significantly increase in task-induced entropy. In our study, PDMs were found to exhibit loss of complexity in pain-related brain regions. Complexity has been reported to reflect the increase of transitions between stable and synchronous microstates through neuronal reentrant loops [116]. We speculate that the loss of complexity in PDMs could be attributed to the chronic stress elicited by recurrent menstrual pain. In our previous structural brain study, gray matter volume loss in regions of pain transmission, sensory processing, and affect regulation was found in PDMs [17]. Two resting-state fMRI studies reported trait-related hypoconnectivity between DMN and salience network during non-painful state [13,24]. The loss of complexity in PDMs may result from inter-regional structural disconnections or decreased neuronal coupling interactions, and the possible underlying mechanisms include loss of neurons [17] or loss of local connectivity [13,24].

4.2. Clinical Implications of Altered Brain Complexity at Rest in Chronic Pain

In this study, PDMs demonstrated loss of complexity in considerable pain-related brain regions (Table 3), including regions in the default-mode network (DMN), limbic regions, sensorimotor network (SMN), and salience network (SAN) compared to healthy female controls.

DMN, ECN, SMN, and SAN are largely influenced by chronic pain experiences [24,117,118] and are highly interactive with the descending pain modulatory system [24]. In healthy individuals, DMN emerges at rest, mainly deactivated towards stimuli or task [117], and has also been reported to involve in the modulation of pain experience [118]. In our previous resting-state fMRI connectivity study, trait-related hypoconnectivity between DMN and salience network was observed during non-painful state [24]. Loss of complexity in the DMN regions in PDMs, even during pain-free state, may add to prior research findings in resting-state fMRI pain studies that reveal decreased functional connectivity of the anterior to posterior parts of DMN in chronic pain patients [24,118], indicating a maladaptive state in chronic pain patients. In addition, hemispheric asymmetry of brain complexity and spectral features in the anterior parts of DMN differed significantly between PDMs and CONs, implying that differences in the hemispheric asymmetry pattern might provide additional neurophysiological information related to chronic pain [26,119,120].

The hippocampus and parahippocampal gyrus, though located in the limbic region, are also regarded as core regions associated with DMN [89]. Hippocampus is substantially involved in emotional learning, and parahippocampal gyrus is thought to be involved in stress-related disorders

and anticipatory anxiety [121]. As long-term menstrual pain serves as a chronic stressor in life, this explains that the asymmetry of brain complexity in the parahippocampal gyrus was found to be positively associated with anxiety level in PDMs in this study. Brain complexity in the left thalamus and the right hippocampus were positively associated with depression level. On the other hand, the amygdala is a well-known region related to the affective-motivational dimension of pain [122] and shows altered resting-state activities in chronic pain conditions [123]. The complexity of the amygdala was also found to be decreased in PDMs in this study, implying that emotional processing could be altered.

In this study, loss of complexity was found in the sensorimotor regions, including the thalamus and Rolandic operculum, in PDMs. Sensorimotor network (SMN) is involved in the processing of sensory-discriminative dimension of pain. Cross-network functional connectivity in the sensorimotor cortex is associated with measures of physical function and is influenced by chronic pain [117]. Thalamus, in particular, is a key region in ascending pain modulatory system that transmits sensory/nociceptive stimuli to cerebral and has reciprocal connections with cerebral cortex [124]. Our results support the evidence that indicates damage in thalamus leads to severe chronic pain [124].

In contrast, activity in salience network is normally anticorrelated with that in DMN [117]. Anterior cingulate cortex (ACC) engages in the emotional/motivational component of pain perception [125,126] and is a key region in the salience network (SAN) [102], which is activated when we constantly engage and focus on the pain but is normally deactivated when pain is gone. In a structural brain study [17], the gray matter volume of ACC was found to be increased in PDMs. We found that MSE in ACC is higher in PDMs compared to that in healthy controls, which suggest excessive attention processing of potential pain salience even in the absence of pain. Together with the negative findings in the between-group grand-averaged MSE global and network-wise tests, our findings suggest that brain complexity of PDM females does not alter globally or systematically, but at specific brain regions at some temporal scales.

4.3. Entropy with Multiple Scales Corresponding to Various Ranges of Frequency

Previous studies have found distinct results for different scales in MSE and suggested that a single scale is not enough for the analysis of biological signals [36,38,40,54,113,127,128]. However, the interpretation of the biological mechanisms reflected by multiple scales has not been well-established. A known fact is that there is a close relationship between the temporal scales in MSE and the frequencies of the signals: the small scale (fine scales) factors reflect the complexity of oscillations at higher frequencies whereas larger scale (coarse scales) factors reflect those at lower frequencies [43,46,129]. Recently, Courtiol et al. [129] have used simulated white noises and experimental EEG data to investigate how the values of MSE across different scales change along with different power spectra of the signals. The procedure of temporal averaging in MSE can be regarded as performing downsampling or low-pass filtering on the original signals. Therefore, according to Nyquist-Shannon's sampling theorem, the MSE at scale factors can detect the irregularity of signals with frequencies less than $(f_s/\tau)/2$, where f_s is the sampling rate of the original signals. Previous studies have linked the signals with high frequencies to information processing in local region whereas those with low frequencies to long-range communication between brain regions [46,130]. Together with the previous findings that the entropy of brain signals reflects the information processing in the brain, it is possible that MSE at different temporal scales may reveal the brain dynamics with different spatial scales [129]. Power spectral analyses in chronic pain patients at rest suggests an increased EEG power in lower frequency bands, including theta and alpha bands [131,132]. In our previous study, we also successfully predicted current pain level in PDMs during menstruation using low frequency components [26]. In this study, MSE group differences only emerged at large scale factors ($\tau = 52\sim 100$), approximately below 10 Hz, implicating that the loss of complexity in PDMs might be related to dysfunction of the distributed/global processing and inter-region communication in the brain after long-term pain experience.

4.4. MSE Versus Spectral Analyses

Increased theta, alpha, beta, or delta band power in chronic pain patients at rest has been reported [131]. In our recent study, the combination of MSE and spectral features could accurately predict current pain intensity in PDMs during painful menstruation [26]. The present study further extends the MSE and spectral analyses to capture brain complexity alterations shaped by long-term menstrual pain during non-painful state. The possible explanations of the findings that MSE features revealed more differences than spectral features might be due to the symptoms of PDM and the study state (pain-free state). First, primary dysmenorrhea, as regarded as “primary” [2], is a chronic pain syndrome without identified structural lesion or anomaly in the affected area (female genital organs). Other chronic pain disorders that involved tissue damage or systemic symptoms, such as chronic low back pain (CLBP) and fibromyalgia, might suffer from constant peripheral nociceptive feedbacks [122] and are thus more likely to show systemic and rhythmic changes in central nervous system that can be captured by linear analyses, such as spectral analysis. Second, although PDMs do suffer from significant negative cognitive and emotional consequences when compared to healthy females including depression, anxiety [7,11], they are considered as otherwise-healthy females who do not suffer from cognitive impairments or mental dysfunctions. This is reasonable to consider that local linear synchrony neural activities in PDMs are similar to those in CONs when spontaneous pain (menstrual pain) does not exist. On the other hand, MSE can effectively capture distributed and long-range dynamics mixed by different brain regions and time scales.

4.5. Limitations

There are some limitations in the present study. First, regional features of MSE were defined using an automated anatomical labeling (AAL) template, which is relatively coarse in spatial resolution comparing to voxel-wise analyses. Second, other MSE measures [38,39] could be used to explore brain complexity in chronic pain. Finally, categorization and nomenclature of the resting-state networks vary across different studies, thereby warrant cautious interpretation of their functions.

5. Conclusions

The brain encompasses both regular and irregular neuronal activities interacting at different spatial and temporal scales. Pain chronicity leads to functional neuroplasticity changes and structural reorganizations, yet the neural complexity, which is reflected by the moment-to-moment temporal variability of nonlinear neural activities, altered by chronic pain is understudied. In this study, we investigated the resting-state magnetoencephalographic signals during pain-free state in 80 PDMs with long-term menstrual pain history and 76 CONs. Revealed by multiscale sample entropy (MSE), PDMs exhibited loss of brain complexity in pain-related brain regions including regions in the default-mode network, limbic circuits, sensorimotor network, and salience network. Significant correlations between MSE values and psychological states (depression and anxiety) found in PDMs may indicate specific nonlinear disturbances in limbic and default mode network circuits after long-term menstrual pain. Our findings suggest that MSE is an important measure of brain complexity and is potentially applicable to future diagnosis of chronic pain.

Supplementary Materials: The following are available online at www.mdpi.com/1099-4300/19/12/680/s1, Table S1: Reported RSNs of each AAL brain regions. Table S2: Lateralization of MSE within PDM and CON groups sorted by scale factor intervals and hemispheric asymmetry alteration in PDM. Table S3: Lateralization of MSE within PDM and CON groups sorted by hemispheric asymmetry alteration in PDM and brain region. Table S4: Lateralization of spectral features within PDM and CON groups.

Acknowledgments: This study was supported in part by grants from Ministry of Science Technology (NSC-102-2629-B-010-001, MOST-104-2410-H-010-004-MY2, MOST-105-2221-E-009-057, MOST-105-2321-B-010-002, MOST-106-2420-H-009-001, MOST-106-2218-E-010-004-MY3), Taipei Veterans General Hospital (V100D-001, V104C-127), TVGH-NTUH joint research program (VN103-05, VN104-03), and Integrated Brain Research Unit, Department of Medical Research, Taipei Veterans General Hospital. We appreciate the assistance of Wei-Chi Li, Ian-Ting Chu, Ching-Ju Yang, Tzi-Ling Tzeng, Chih-Ying Chuang, Chih-Cher Chou, Lin-Chien Lee, Yu-Mei Chang,

Chiu-Jung Huang, Ruei-Jyun Hung, Yi-Jun Liu, and Li-Kai Cheng with participant recruitment and MEG/MRI experiments. All participants are thanked for their support and contribution to this study.

Author Contributions: Li-Fen Chen and Jen-Chuen Hsieh conceived and designed the experiments; Intan Low and Yu-Hsiang Liu performed the experiments; Hsiang-Tai Chao performed the clinical assessment; Po-Chih Kuo and Yong-Sheng Chen developed the methodology; Yu-Hsiang Liu, Cheng-Lin Tsai and Intan Low analyzed the data; Jen-Chuen Hsieh provided substantial intellectual input for the work; Intan Low, Po-Chih Kuo, Yong-Sheng Chen and Li-Fen Chen wrote the manuscript. All authors have read and approved the final manuscript.

Conflicts of Interest: The authors declare no conflict of interest.

Appendix A

The analysis of Lempel-Ziv complexity (LZC) [81] is based on a finite symbol sequence, so the given signal must be coarse-grained by transforming it into a sequence with only a few symbols. In this study, we binarized the time series of the cortical source activity into a binary sequence by comparing sample points with the threshold T_d . The original time series is converted to a binary sequence $P = [s_1, s_2, \dots, s_N]$, where s_i is defined by:

$$s_i = \begin{cases} 0, & \text{if } x_i < T_d \\ 1, & \text{otherwise} \end{cases} \quad (\text{A1})$$

The value T_d was assigned as the median of the time series in this study due to median is insensitive to outliers [133].

To compute the LZC of sequence P , sequence P was scanned from left to right. Whenever a new subsequence was found, complexity counter $c(N)$ would be increased by one unit. The algorithm of LZC is as follows:

Let S and Q denote the subsequences of the sequence P , and SQ denote the cascade of S and Q . The expression π denotes the operation used to remove the last symbols in a sequence. Therefore, subsequence $SQ\pi$ is derived from the removal of the last symbol of SQ . The expression $v(SQ\pi)$ denotes the set which contains all different subsequences of $SQ\pi$.

To begin with, we assign the initial values of $c(N) = 1$, $S = s_1$, $Q = s_2$, and $SQ\pi = s_1$, and to be general, we suppose $S = s_1, s_2, \dots, s_r$, $Q = s_{r+1}, s_{r+2}, \dots, s_{r+i}$, and $SQ\pi = s_1, s_2, \dots, s_r, s_{r+1}, \dots, s_{r+i-1}$. While P is being scanned from left to right, either of the two conditions may occurs:

If $Q \in v(SQ\pi)$, then Q is a subsequence of $SQ\pi$, namely, Q is not a new sequence, so SQ can be extended from S by recursive copying a certain subsequence of S [134]. In this case, S is unchanged, and Q is renewed to be $s_{r+1}, s_{r+2}, \dots, s_{r+i}, s_{r+i+1}$.

If $Q \notin v(SQ\pi)$, then Q is not a subsequence of $SQ\pi$ but a newly emerging sequence, namely, SQ cannot be extended from S by recursive copying a certain subsequence of S . In this case, increase $c(N)$ by one, renew S with the concatenation of S and Q , and renew Q with s_{r+i+1} . At this time, S is $s_1, s_2, \dots, s_r, s_{r+1}, \dots, s_{r+i}$ and Q is s_{r+i+1} .

Repeat the previously mentioned procedure until Q involves the last symbol of the sequence P , and in the meantime, the complexity counter $c(N)$ is the LZC measure. The last step is to normalize $c(N)$ by the upper bound of $c(N)$ [81] which is written below:

$$\lim_{N \rightarrow \infty} c(N) = b(N) = \frac{N}{\log_{\alpha} N} \quad (\text{A2})$$

For a binary sequence, $\alpha = 2$:

$$b(N) = \frac{N}{\log_2 N} \quad (\text{A3})$$

and the normalized $c(N)$ is:

$$C(N) = \frac{c(N)}{b(N)} \quad (\text{A4})$$

The normalized LZC $C(N)$ can be regarded as the occurrence frequency of new patterns along with the sequence [135].

References

1. Merskey, H.; Bogduk, N. *Classification of Chronic Pain: Descriptions of Chronic Pain Syndromes and Definitions of Pain Terms*, 2nd ed.; Harold Merskey, N.B., Ed.; IASP Press: Seattle, WA, USA, 2002.
2. Treede, R.-D.; Rief, W.; Barke, A.; Aziz, Q.; Bennett, M.I.; Benoliel, R.; Cohen, M.; Evers, S.; Finnerup, N.B.; First, M.B.; et al. A classification of chronic pain for ICD-11. *Pain* **2015**, *156*, 1003–1007. [[CrossRef](#)] [[PubMed](#)]
3. Baliki, M.N.; Schnitzer, T.J.; Bauer, W.R.; Apkarian, A.V. Brain morphological signatures for chronic pain. *PLoS ONE* **2011**, *6*, e26010. [[CrossRef](#)]
4. Smith, D.; Wilkie, R.; Uthman, O.; Jordan, J.L.; McBeth, J. Chronic pain and mortality: A systematic review. *PLoS ONE* **2014**, *9*, e99048.
5. Coco, A.S. Primary dysmenorrhea. *Am. Fam. Phys.* **1999**, *60*, 489–496.
6. Dawood, M.Y. Primary Dysmenorrhea: Advances in Pathogenesis and Management. *Obstet. Gynecol.* **2006**, *108*, 428–441. [[CrossRef](#)] [[PubMed](#)]
7. Iacovides, S.; Avidon, I.; Baker, F.C. What we know about primary dysmenorrhea today: A critical review. *Hum. Reprod. Updat.* **2015**, *21*, 762–778. [[CrossRef](#)] [[PubMed](#)]
8. Dawood, M.Y. Dysmenorrhea. *J. Reprod. Med.* **1985**, *30*, 154–167. [[PubMed](#)]
9. Proctor, M.L.; Smith, C.A.; Farquhar, C.M.; Stones, R.W. Transcutaneous electrical nerve stimulation and acupuncture for primary dysmenorrhoea. *Cochrane Database Syst. Rev.* **2002**, CD002123. [[CrossRef](#)]
10. IASP Taxonomy Working Group. Visceral and Other Syndromes of the Trunk Apart from Spinal and Radicular Pain. Classification of Chronic Pain, 2nd Edition (Revised). Available online: https://www.iasp-pain.org/files/Content/ContentFolders/Publications2/ClassificationofChronicPain/Part_II-F.pdf (accessed on 12 September 2017).
11. Lee, L.-C.; Tu, C.-H.; Chen, L.-F.; Shen, H.-D.; Chao, H.-T.; Lin, M.-W.; Hsieh, J.-C. Association of brain-derived neurotrophic factor gene VAL66MET polymorphism with primary dysmenorrhea. *PLoS ONE* **2014**, *9*, e112766. [[CrossRef](#)]
12. Balık, G.; Ustüner, I.; Kağıtçı, M.; Sahin, F.K. Is there a relationship between mood disorders and dysmenorrhea? *J. Pediatr. Adolesc. Gynecol.* **2014**, *27*, 371–374. [[CrossRef](#)] [[PubMed](#)]
13. Wei, S.-Y.; Chao, H.-T.; Tu, C.-H.; Li, W.-C.; Low, I.; Chuang, C.-Y.; Chen, L.-F.; Hsieh, J.-C. Changes in functional connectivity of pain modulatory systems in women with primary dysmenorrhea. *Pain* **2015**, *157*, 1. [[CrossRef](#)] [[PubMed](#)]
14. Staud, R. Abnormal endogenous pain modulation is a shared characteristic of many chronic pain conditions. *Expert Rev. Neurother.* **2012**, *12*, 577–585. [[CrossRef](#)] [[PubMed](#)]
15. Li, W.C.; Tu, C.H.; Chao, H.T.; Yeh, T.C.; Chen, L.F.; Hsieh, J.C. High prevalence of incidental brain findings in primary dysmenorrhoea. *Eur. J. Pain* **2015**, *19*, 1071–1074. [[CrossRef](#)] [[PubMed](#)]
16. Liu, P.; Yang, J.; Wang, G.; Liu, Y.; Liu, X.; Jin, L.; Liang, F.; Qin, W.; Calhoun, V.D. Altered regional cortical thickness and subcortical volume in women with primary dysmenorrhoea. *Eur. J. Pain* **2016**, *20*, 512–520. [[CrossRef](#)] [[PubMed](#)]
17. Tu, C.H.; Niddam, D.M.; Chao, H.T.; Chen, L.F.; Chen, Y.S.; Wu, Y.T.; Yeh, T.C.; Lirng, J.F.; Hsieh, J.C. Brain morphological changes associated with cyclic menstrual pain. *Pain* **2010**, *150*, 462–468. [[CrossRef](#)]
18. Tu, C.-H.; Niddam, D.M.; Yeh, T.-C.; Lirng, J.-F.; Cheng, C.-M.; Chou, C.-C.; Chao, H.-T.; Hsieh, J.-C. Menstrual pain is associated with rapid structural alterations in the brain. *Pain* **2013**, *154*, 1718–1724. [[CrossRef](#)] [[PubMed](#)]
19. Liu, P.; Liu, Y.; Wang, G.; Li, R.; Wei, Y.; Fan, Y.; Yu, Y.; Deng, D.; Qin, W. Changes of functional connectivity of the anterior cingulate cortex in women with primary dysmenorrhea. *Brain Imaging Behav.* **2017**, 1–8. [[CrossRef](#)] [[PubMed](#)]
20. Tu, C.H.; Niddam, D.M.; Chao, H.T.; Liu, R.S.; Hwang, R.J.; Yeh, T.C.; Hsieh, J.C. Abnormal cerebral metabolism during menstrual pain in primary dysmenorrhea. *Neuroimage* **2009**, *47*, 28–35. [[CrossRef](#)] [[PubMed](#)]
21. Vincent, K.; Warnaby, C.; Stagg, C.J.; Moore, J.; Kennedy, S.; Tracey, I. Dysmenorrhoea is associated with central changes in otherwise healthy women. *Pain* **2011**, *152*, 1966–1975. [[CrossRef](#)] [[PubMed](#)]

22. Wei, S.-Y.; Chao, H.-T.; Tu, C.-H.; Lin, M.-W.; Li, W.-C.; Low, I.; Shen, H.-D.; Chen, L.-F.; Hsieh, J.-C. The BDNF Val66Met polymorphism is associated with the functional connectivity dynamics of pain modulatory systems in primary dysmenorrhea. *Sci. Rep.* **2016**, *6*, 23639. [[CrossRef](#)] [[PubMed](#)]
23. Wei, S.-Y.; Chen, L.-F.; Lin, M.-W.; Li, W.-C.; Low, I.; Yang, C.-J.; Chao, H.-T.; Hsieh, J.-C. The OPRM1 A118G polymorphism modulates the descending pain modulatory system for individual pain experience in young women with primary dysmenorrhea. *Sci. Rep.* **2017**, *7*, 39906. [[CrossRef](#)] [[PubMed](#)]
24. Wu, T.-H.; Tu, C.-H.; Chao, H.-T.; Li, W.-C.; Low, I.; Chuang, C.-Y.; Yeh, T.-C.; Cheng, C.-M.; Chou, C.-C.; Chen, L.-F.; et al. Dynamic changes of functional pain connectome in women with primary dysmenorrhea. *Sci. Rep.* **2016**, *6*, 24543. [[CrossRef](#)] [[PubMed](#)]
25. Zhang, B.; Xu, Y.; He, W.; Wang, J.; Chai, H.; Shen, C.; Zhu, Q.; Wang, W.; Beales, D.; Wutzler, A.; et al. Intensity dependence of auditory evoked potentials in primary dysmenorrhea. *J. Pain* **2017**, *151*, 27–43. [[CrossRef](#)] [[PubMed](#)]
26. Kuo, P.C.; Chen, Y.T.; Chen, Y.S.; Chen, L.F. Decoding the perception of endogenous pain from resting-state MEG. *Neuroimage* **2017**, *144*, 1–11. [[CrossRef](#)] [[PubMed](#)]
27. Stam, C.J. Nonlinear dynamical analysis of EEG and MEG: Review of an emerging field. *Clin. Neurophysiol.* **2005**, *116*, 2266–2301. [[CrossRef](#)] [[PubMed](#)]
28. McDonough, I.M.; Nashiro, K.; Nagarajan, S.S.; Chang, C.; Gorgolewski, K. Network complexity as a measure of information processing across resting-state networks: Evidence from the Human Connectome Project. *Front. Hum. Neurosci.* **2014**, *8*, 1–15. [[CrossRef](#)] [[PubMed](#)]
29. Tononi, G.; Sporns, O.; Edelman, G.M. A measure for brain complexity: Relating functional segregation and integration in the nervous system. *Proc. Natl. Acad. Sci. USA* **1994**, *91*, 5033–5037. [[CrossRef](#)] [[PubMed](#)]
30. Friston, K.J. The labile brain. I. Neuronal transients and nonlinear coupling. *Philos. Trans. R. Soc. Lond. Ser. B Biol. Sci.* **2000**, *355*, 215–236. [[CrossRef](#)] [[PubMed](#)]
31. Friston, K.J. The labile brain. II. Transients, complexity and selection. *Philos. Trans. R. Soc. Lond. B Biol. Sci.* **2000**, *355*, 237–252. [[CrossRef](#)] [[PubMed](#)]
32. Nakagawa, T.T.; Jirsa, V.K.; Spiegler, A.; McIntosh, A.R.; Deco, G. Bottom up modeling of the connectome: Linking structure and function in the resting brain and their changes in aging. *Neuroimage* **2013**, *80*, 318–329. [[CrossRef](#)] [[PubMed](#)]
33. Garrett, D.D.; Samanez-Larkin, G.R.; MacDonald, S.W.S.; Lindenberger, U.; McIntosh, A.R.; Grady, C.L. Moment-to-moment brain signal variability: A next frontier in human brain mapping? *Neurosci. Biobehav. Rev.* **2013**, *37*, 610–624. [[CrossRef](#)] [[PubMed](#)]
34. Richman, J.S.; Moorman, J.R. Physiological time-series analysis using approximate entropy and sample entropy. *Am. J. Physiol. Heart. Circ. Physiol.* **2000**, *278*, H2039–H2049. [[CrossRef](#)] [[PubMed](#)]
35. Yang, A.C.; Tsai, S.-J. Is mental illness complex? From behavior to brain. *Prog. Neuro-Psychopharmacol. Biol. Psychiatry* **2013**, *45*, 253–257. [[CrossRef](#)]
36. Costa, M.; Goldberger, A.L.; Peng, C.-K. Multiscale entropy analysis of complex physiologic time series. *Phys. Rev. Lett.* **2002**, *89*, 6–9. [[CrossRef](#)] [[PubMed](#)]
37. Costa, M.; Goldberger, A.L.; Peng, C.K. Multiscale entropy analysis of biological signals. *Phys. Rev. E* **2005**, *71*, 1–18. [[CrossRef](#)] [[PubMed](#)]
38. Hu, M.; Liang, H. Multiscale Entropy: Recent Advances. In *Complexity and Nonlinearity in Cardiovascular Signals*; Springer International Publishing: Cham, Switzerland, 2017; pp. 115–138.
39. Humeau-Heurtier, A. The multiscale entropy algorithm and its variants: A review. *Entropy* **2015**, *17*, 3110–3123. [[CrossRef](#)]
40. Park, J.-H.; Kim, S.; Kim, C.-H.; Cichocki, A.; Kim, K. Multiscale entropy analysis of EEG from patients under different pathological conditions. *Fractals* **2007**, *15*, 399. [[CrossRef](#)]
41. Heisz, J.J.; McIntosh, A.R. Applications of EEG neuroimaging data: Event-related potentials, spectral power, and multiscale entropy. *J. Vis. Exp.* **2013**, 1–8. [[CrossRef](#)] [[PubMed](#)]
42. Yang, A.C.; Wang, S.J.; Lai, K.L.; Tsai, C.F.; Yang, C.H.; Hwang, J.P.; Lo, M.T.; Huang, N.E.; Peng, C.K.; Fuh, J.L. Cognitive and neuropsychiatric correlates of EEG dynamic complexity in patients with Alzheimer's disease. *Prog. Neuro-Psychopharmacol. Biol. Psychiatry* **2013**, *47*, 52–61. [[CrossRef](#)] [[PubMed](#)]
43. Takahashi, T.; Cho, R.Y.; Mizuno, T.; Kikuchi, M.; Murata, T.; Takahashi, K.; Wada, Y. Antipsychotics reverse abnormal EEG complexity in drug-naive schizophrenia: A multiscale entropy analysis. *Neuroimage* **2010**, *51*, 173–182. [[CrossRef](#)] [[PubMed](#)]

44. Liu, Q.; Chen, Y.F.; Fan, S.Z.; Abbod, M.F.; Shieh, J.S. EEG artifacts reduction by multivariate empirical mode decomposition and multiscale entropy for monitoring depth of anaesthesia during surgery. *Med. Biol. Eng. Comput.* **2017**, *55*, 1435–1450. [[CrossRef](#)] [[PubMed](#)]
45. Liu, Q.; Wei, Q.; Fan, S.Z.; Lu, C.W.; Lin, T.Y.; Abbod, M.F.; Shieh, J.S. Adaptive computation of multiscale entropy and its application in EEG signals for monitoring depth of anesthesia during surgery. *Entropy* **2012**, *14*, 978–992. [[CrossRef](#)]
46. Mizuno, T.; Takahashi, T.; Cho, R.Y.; Kikuchi, M.; Murata, T.; Takahashi, K.; Wada, Y. Assessment of EEG dynamical complexity in Alzheimer’s disease using multiscale entropy. *Clin. Neurophysiol.* **2010**, *121*, 1438–1446. [[CrossRef](#)] [[PubMed](#)]
47. Hornero, R.; Abasolo, D.; Escudero, J.; Gomez, C. Nonlinear analysis of electroencephalogram and magnetoencephalogram recordings in patients with Alzheimer’s disease. *Philos. Trans. R. Soc. A Math. Phys. Eng. Sci.* **2009**, *367*, 317–336. [[CrossRef](#)] [[PubMed](#)]
48. Jaworska, N.; Wang, H.; Smith, D.M.; Blier, P.; Knott, V.; Protzner, A.B. Pre-treatment EEG signal variability is associated with treatment success in depression. *NeuroImage Clin.* **2018**, *17*, 368–377. [[CrossRef](#)] [[PubMed](#)]
49. Grandy, T.H.; Garrett, D.D.; Schmiedek, F.; Werkle-Bergner, M. On the estimation of brain signal entropy from sparse neuroimaging data. *Sci. Rep.* **2016**, *6*, 23073. [[CrossRef](#)] [[PubMed](#)]
50. Polizzotto, N.R.; Takahashi, T.; Walker, C.P.; Cho, R.Y. Wide range multiscale entropy changes through development. *Entropy* **2016**, *18*. [[CrossRef](#)]
51. Catarino, A.; Churches, O.; Baron-Cohen, S.; Andrade, A.; Ring, H. Atypical EEG complexity in autism spectrum conditions: A multiscale entropy analysis. *Clin. Neurophysiol.* **2011**, *122*, 2375–2383. [[CrossRef](#)] [[PubMed](#)]
52. McIntosh, A.R.; Kovacevic, N.; Itier, R.J. Increased Brain Signal Variability Accompanies Lower Behavioral Variability in Development. *PLoS Comput. Biol.* **2008**, *4*, e1000106. [[CrossRef](#)] [[PubMed](#)]
53. Sitges, C.; Bornas, X.; Llabrés, J.; Noguera, M.; Montoya, P. Linear and nonlinear analyses of EEG dynamics during non-painful somatosensory processing in chronic pain patients. *Int. J. Psychophysiol.* **2010**, *77*, 176–183. [[CrossRef](#)] [[PubMed](#)]
54. Takahashi, T.; Cho, R.Y.; Murata, T.; Mizuno, T.; Kikuchi, M.; Mizukami, K.; Kosaka, H.; Takahashi, K.; Wada, Y. Age-related variation in EEG complexity to photic stimulation: A multiscale entropy analysis. *Clin. Neurophysiol.* **2009**, *120*, 476–483. [[CrossRef](#)] [[PubMed](#)]
55. Wang, C.H.; Tsai, C.L.; Tseng, P.; Yang, A.C.; Lo, M.T.; Peng, C.K.; Wang, H.Y.; Muggleton, N.G.; Juan, C.H.; Liang, W.K. The association of physical activity to neural adaptability during visuo-spatial processing in healthy elderly adults: A multiscale entropy analysis. *Brain Cogn.* **2014**, *92*, 73–83. [[CrossRef](#)] [[PubMed](#)]
56. Hornero, R.; Escudero, J.; Fernández, A.; Poza, J.; Gómez, C. Spectral and nonlinear analyses of MEG background activity in patients with Alzheimer’s disease. *IEEE Trans. Biomed. Eng.* **2008**, *55*, 1658–1665. [[CrossRef](#)] [[PubMed](#)]
57. Hu, P.-C.; Kuo, P.-C.; Chen, L.-F.; Chen, Y.-S. Objective assessment of menstrual pain scale from resting brain signals. In *Digest of Technical Papers—IEEE International Conference on Consumer Electronics*; IEEE: New York, NY, USA, 2014; pp. 167–168.
58. Brookes, M.J.; Hall, E.L.; Robson, S.E.; Price, D.; Palaniyappan, L.; Liddle, E.B.; Liddle, P.F.; Robinson, S.E.; Morris, P.G. Complexity measures in magnetoencephalography: Measuring “disorder” in schizophrenia. *PLoS ONE* **2015**, *10*, e0120991. [[CrossRef](#)] [[PubMed](#)]
59. Misić, B.; Mills, T.; Taylor, M.J.; McIntosh, A.R. Brain noise is task dependent and region specific. *J. Neurophysiol.* **2010**, *104*, 2667–2676. [[CrossRef](#)] [[PubMed](#)]
60. Yang, A.C.; Huang, C.C.; Yeh, H.L.; Liu, M.E.; Hong, C.J.; Tu, P.C.; Chen, J.F.; Huang, N.E.; Peng, C.K.; Lin, C.P.; et al. Complexity of spontaneous BOLD activity in default mode network is correlated with cognitive function in normal male elderly: A multiscale entropy analysis. *Neurobiol. Aging* **2013**, *34*, 428–438. [[CrossRef](#)] [[PubMed](#)]
61. Yang, A.C.; Hong, C.J.; Liou, Y.J.; Huang, K.L.; Huang, C.C.; Liu, M.E.; Lo, M.T.; Huang, N.E.; Peng, C.K.; Lin, C.P.; et al. Decreased resting-state brain activity complexity in schizophrenia characterized by both increased regularity and randomness. *Hum. Brain Mapp.* **2015**, *36*, 2174–2186. [[CrossRef](#)] [[PubMed](#)]
62. Goldberger, A.L.; Peng, C.K.; Lipsitz, L.A. What is physiologic complexity and how does it change with aging and disease? *Neurobiol. Aging* **2002**, *23*, 23–26. [[CrossRef](#)]

63. Hager, B.; Yang, A.C.; Brady, R.; Meda, S.; Clementz, B.; Pearlson, G.D.; Sweeney, J.A.; Tamminga, C.; Keshavan, M. Neural complexity as a potential translational biomarker for psychosis. *J. Affect. Disord.* **2017**, *216*, 89–99. [[CrossRef](#)] [[PubMed](#)]
64. Poza, J.; Hornero, R.; Abásolo, D.; Fernández, A.; García, M. Extraction of spectral based measures from MEG background oscillations in Alzheimer's disease. *Med. Eng. Phys.* **2007**, *29*, 1073–1083. [[CrossRef](#)] [[PubMed](#)]
65. Escudero, J.; Abásolo, D.; Hornero, R.; Espino, P.; López, M. Analysis of electroencephalograms in Alzheimer's disease patients with multiscale entropy. *Physiol. Meas.* **2006**, *27*, 1091–1106. [[CrossRef](#)] [[PubMed](#)]
66. Melzack, R. The McGill Pain Questionnaire: Major properties and scoring methods. *Pain* **1975**, *1*, 277–299. [[CrossRef](#)]
67. Melzack, R. *The McGill Pain Questionnaire. Pain Measurement and Assessment*; Raven Press: New York, NY, USA, 1983; ISBN 978-0-89-004893-1.
68. Tseng, H.M.; Lu, J.F.; Gandek, B. Cultural issues in using the SF-36 Health Survey in Asia: Results from Taiwan. *Heal. Qual. Life Outcomes* **2003**, *1*, 72. [[CrossRef](#)] [[PubMed](#)]
69. Ware, J.E.; Snow, K.K.; Kosinski, M.; Gandek, B. *SF-36 Health Survey: Manual and Interpretation Guide*; Health Institute, Tufts Medical Center: Boston, MA, USA, 1993.
70. Holden, R.R.; Fekken, G.C.; Reddon, J.R.; Helmes, E.; Jackson, D.N. Clinical reliabilities and validities of the Basic Personality Inventory. *J. Consult. Clin. Psychol.* **1988**, *56*, 766–768. [[CrossRef](#)] [[PubMed](#)]
71. Spielberger, C.D.; Gorsuch, R.L.; Lushene, R.; Vagg, P.R.; Jacobs, G.A. *Manual for the State-Trait Anxiety Inventory (form Y)*; Consulting Psychologists Press: Palo Alto, CA, USA, 1983.
72. Beck, A.T.; Rush, A.J.; Shaw, B.F.; Emery, G. *Cognitive Therapy of Depression*; Guilford Press: New York, NY, USA, 1979; ISBN 0-898-62919-5.
73. Beck, A.T.; Steer, R.A. *Manual for the Beck Anxiety Inventory*; Psychological Corporation: San Antonio, TX, USA, 1993.
74. Sullivan, M.J.; Bishop, S.P.J. The pain catastrophizing scale: Development and validation. *Psychol. Assess.* **1995**, *7*, 524–532. [[CrossRef](#)]
75. Uusitalo, M.A.; Ilmoniemi, R.J. Signal-space projection method for separating MEG or EEG into components. *Med. Biol. Eng. Comput.* **1997**, *35*, 135–140. [[CrossRef](#)] [[PubMed](#)]
76. Chen, Y.S.; Cheng, C.Y.; Hsieh, J.C.; Chen, L.F. Maximum contrast beamformer for electromagnetic mapping of brain activity. *IEEE Trans. Biomed. Eng.* **2006**, *53*, 1765–1774. [[CrossRef](#)] [[PubMed](#)]
77. Tikhonov, A.N.; Arsenin, V.Y. *Solution of Ill-Posed Problems*; Scripta Series in Mathematics; VH Winston: Washington, DC, USA, 1977; ISBN 0-470-99124-0.
78. Pincus, S.; Goldberger, A. Physiological time-series analysis: What does regularity quantify? *Am. J. Physiol.* **1994**, *266*, H1643–H1656. [[PubMed](#)]
79. McIntosh, A.R.; Vakorin, V.; Kovacevic, N.; Wang, H.; Diaconescu, A.; Protzner, A.B. Spatiotemporal dependency of age-related changes in brain signal variability. *Cereb. Cortex* **2014**, *24*, 1806–1817. [[CrossRef](#)] [[PubMed](#)]
80. Shannon, C.E. A mathematical theory of communication. *Bell Syst. Tech. J.* **1948**, *27*, 379–423. [[CrossRef](#)]
81. Lempel, A.; Ziv, J. On the Complexity of Finite Sequences. *IEEE Trans. Inf. Theory* **1976**, *22*, 75–81. [[CrossRef](#)]
82. Schwender, D.; Dauderer, M.; Mulzer, S.; Klasing, S.; Finsterer, U.; Peter, K. Spectral edge frequency of the electroencephalogram to monitor “depth” of anaesthesia with isoflurane or propofol. *Br. J. Anaesth.* **1996**, *77*, 179–184. [[CrossRef](#)] [[PubMed](#)]
83. Tzourio-Mazoyer, N.; Landeau, B.; Papathanassiou, D.; Crivello, F.; Etard, O.; Delcroix, N.; Mazoyer, B.; Joliot, M. Automated anatomical labeling of activations in SPM using a macroscopic anatomical parcellation of the MNI MRI single-subject brain. *Neuroimage* **2002**, *15*, 273–289. [[CrossRef](#)] [[PubMed](#)]
84. Rorden, C.; Brett, M. Stereotaxic display of Brain lesions. *Behav. Neurol.* **2000**, *12*, 191–200. [[CrossRef](#)] [[PubMed](#)]
85. Alemán-Gómez, Y.; Melie-García, L.; Valdés-Hernandez, P. IBASPM: Toolbox for automatic parcellation of brain structures. In Proceedings of the 12th Annual Meeting of the Organization for Human Brain Mapping, Florence, Italy, 11–15 June 2006.
86. He, Y.; Wang, J.; Wang, L.; Chen, Z.J.; Yan, C.; Yang, H.; Tang, H.; Zhu, C.; Gong, Q.; Zang, Y.; et al. Uncovering intrinsic modular organization of spontaneous brain activity in humans. *PLoS ONE* **2009**, *4*, e5226. [[CrossRef](#)] [[PubMed](#)]

87. Kim, M.J.; Gee, D.G.; Loucks, R.A.; Davis, F.C.; Whalen, P.J. Anxiety Dissociates dorsal and ventral medial prefrontal cortex functional connectivity with the amygdala at rest. *Cereb. Cortex* **2011**, *21*, 1667–1673. [[CrossRef](#)] [[PubMed](#)]
88. Cox, C.L.; Uddin, L.Q.; Dimartino, A.; Castellanos, F.X.; Milham, M.P.; Kelly, C. The balance between feeling and knowing: Affective and cognitive empathy are reflected in the brain's intrinsic functional dynamics. *Soc. Cogn. Affect. Neurosci.* **2012**, *7*, 727–737. [[CrossRef](#)] [[PubMed](#)]
89. Buckner, R.L.; Andrews-Hanna, J.R.; Schacter, D.L. The brain's default network: Anatomy, function, and relevance to disease. *Ann. N. Y. Acad. Sci.* **2008**, *1124*, 1–38. [[CrossRef](#)] [[PubMed](#)]
90. VanDijk, K.R.A.; Hedden, T.; Venkataraman, A.; Evans, K.C.; Lazar, S.W.; Buckner, R.L. Intrinsic functional connectivity as a tool for human connectomics: Theory, properties, and optimization. *J. Neurophysiol.* **2010**, *103*, 297–321. [[CrossRef](#)] [[PubMed](#)]
91. Uddin, L.Q.; Kelly, A.M.C.; Biswal, B.B.; Castellanos, F.X.; Milham, M.P. Functional connectivity of default mode network components: Correlation, anticorrelation, and causality. *Hum. Brain Mapp.* **2009**, *30*, 625–637. [[CrossRef](#)] [[PubMed](#)]
92. Raichle, M.E. The restless brain. *Brain Connect.* **2011**, *1*. [[CrossRef](#)] [[PubMed](#)]
93. Castellanos, F.X.; Proal, E. Large-scale brain systems in ADHD: Beyond the prefrontal-striatal model. *Trends Cogn. Sci.* **2012**, *16*, 17–26. [[CrossRef](#)] [[PubMed](#)]
94. Fox, M.D.; Snyder, A.Z.; Vincent, J.L.; Corbetta, M.; VanEssen, D.C.; Raichle, M.E. The human brain is intrinsically organized into dynamic, anticorrelated functional networks. *Proc. Natl. Acad. Sci. USA* **2005**, *102*, 9673–9678. [[CrossRef](#)] [[PubMed](#)]
95. Fransson, P. Spontaneous low-frequency BOLD signal fluctuations: An fMRI investigation of the resting-state default mode of brain function hypothesis. *Hum. Brain Mapp.* **2005**, *26*, 15–29. [[CrossRef](#)] [[PubMed](#)]
96. Toro, R.; Fox, P.T.; Paus, T. Functional coactivation map of the human brain. *Cereb. Cortex* **2008**, *18*, 2553–2559. [[CrossRef](#)] [[PubMed](#)]
97. Rosazza, C.; Minati, L. Resting-state brain networks: Literature review and clinical applications. *Neurol. Sci.* **2011**, *32*, 773–785. [[CrossRef](#)] [[PubMed](#)]
98. Song, X.W.; Dong, Z.Y.; Long, X.Y.; Li, S.F.; Zuo, X.N.; Zhu, C.Z.; He, Y.; Yan, C.G.; Zang, Y.F. REST: A Toolkit for resting-state functional magnetic resonance imaging data processing. *PLoS ONE* **2011**, *6*, e25031. [[CrossRef](#)] [[PubMed](#)]
99. Tewarie, P.; Schoonheim, M.M.; Stam, C.J.; van derMeer, M.L.; vanDijk, B.W.; Barkhof, F.; Polman, C.H.; Hillebrand, A. Cognitive and clinical dysfunction, altered MEG resting-state networks and thalamic atrophy in multiple sclerosis. *PLoS ONE* **2013**, *8*. [[CrossRef](#)] [[PubMed](#)]
100. Greicius, M.D.; Krasnow, B.; Reiss, A.L.; Menon, V. Functional connectivity in the resting brain: A network analysis of the default mode hypothesis. *Proc. Natl. Acad. Sci. USA* **2003**, *100*, 253–258. [[CrossRef](#)] [[PubMed](#)]
101. Christoff, K.; Irving, Z.C.; Fox, K.C.R.; Spreng, R.N.; Andrews-Hanna, J.R. Mind-wandering as spontaneous thought: A dynamic framework. *Nat. Rev. Neurosci.* **2016**, *17*, 718–731. [[CrossRef](#)] [[PubMed](#)]
102. Seeley, W.W.; Menon, V.; Schatzberg, A.F.; Keller, J.; Glover, G.H.; Kenna, H.; Reiss, A.L.; Greicius, M.D. Dissociable intrinsic connectivity networks for salience processing and executive control. *J. Neurosci.* **2007**, *27*, 2349–2356. [[CrossRef](#)] [[PubMed](#)]
103. Deco, G.; Corbetta, M. The dynamical balance of the brain at rest. *Neuroscientist* **2011**, *17*, 107–123. [[CrossRef](#)] [[PubMed](#)]
104. Spreng, R.N.; Stevens, W.D.; Chamberlain, J.P.; Gilmore, A.W.; Schacter, D.L. Default network activity, coupled with the frontoparietal control network, supports goal-directed cognition. *Neuroimage* **2010**, *53*, 303–317. [[CrossRef](#)] [[PubMed](#)]
105. Niendam, T.A.; Laird, A.R.; Ray, K.L.; Dean, Y.M.; Glahn, D.C.; Carter, C.S. Meta-analytic evidence for a superordinate cognitive control network subserving diverse executive functions. *Cogn. Affect. Behav. Neurosci.* **2012**, *12*, 241–268. [[CrossRef](#)] [[PubMed](#)]
106. Vossel, S.; Geng, J.J.; Fink, G.R. Dorsal and ventral attention systems. *Neuroscience* **2014**, *20*, 150–159. [[CrossRef](#)] [[PubMed](#)]
107. Corbetta, M.; Patel, G.; Shulman, G.L. The reorienting system of the human brain: From environment to theory of mind. *Neuron* **2008**, *58*, 306–324. [[CrossRef](#)] [[PubMed](#)]

108. DeLuca, M.; Beckmann, C.F.; DeStefano, N.; Matthews, P.M.; Smith, S.M. fMRI resting state networks define distinct modes of long-distance interactions in the human brain. *Neuroimage* **2006**, *29*, 1359–1367. [[CrossRef](#)] [[PubMed](#)]
109. Engel, A.K.; Gerloff, C.; Hilgetag, C.C.; Nolte, G. Intrinsic coupling modes: Multiscale interactions in ongoing brain activity. *Neuron* **2013**, *80*, 867–886. [[CrossRef](#)] [[PubMed](#)]
110. Ghasemi, A.; Zahediasl, S. Normality tests for statistical analysis: A guide for non-statisticians. *Int. J. Endocrinol. Metab.* **2012**, *10*, 486–489. [[CrossRef](#)] [[PubMed](#)]
111. Maris, E.; Oostenveld, R. Nonparametric statistical testing of EEG- and MEG-data. *J. Neurosci. Methods* **2007**, *164*, 177–190. [[CrossRef](#)] [[PubMed](#)]
112. Xia, M.; Wang, J.; He, Y. BrainNet Viewer: A network visualization tool for human brain connectomics. *PLoS ONE* **2013**, *8*, e68910. [[CrossRef](#)] [[PubMed](#)]
113. Chung, C.C.; Kang, J.H.; Hu, C.J. Measuring entropy in functional neuroscience: Pathophysiological and clinical applications. *Neurosci. Neuroecon.* **2016**, *5*, 45–53. [[CrossRef](#)]
114. Labate, D.; Foresta, F.L.; Morabito, G.; Palamara, I.; Morabito, F.C. Entropic measures of EEG complexity in alzheimer's disease through a multivariate multiscale approach. *IEEE Sens. J.* **2013**, *13*, 3284–3292. [[CrossRef](#)]
115. Labate, D.; LaForesta, F.; Palamara, I.; Morabito, G.; Bramanti, A.; Zhang, Z.; Morabito, F.C. EEG complexity modifications and altered compressibility in mild cognitive impairment and Alzheimer's Disease. In *Smart Innovation, Systems and Technologies*; Springer: Cham, Switzerland, 2014; Volume 26, pp. 163–173.
116. Friston, K.J. Brain function, nonlinear coupling, and neuronal transients. *Neuroscientist* **2001**, *7*, 406–418. [[CrossRef](#)] [[PubMed](#)]
117. Hemington, K.S.; Wu, Q.; Kucyi, A.; Inman, R.D.; Davis, K.D. Abnormal cross-network functional connectivity in chronic pain and its association with clinical symptoms. *Brain Struct. Funct.* **2016**, *221*, 4203–4219. [[CrossRef](#)] [[PubMed](#)]
118. Baliki, M.N.; Mansour, A.R.; Baria, A.T.; Apkarian, A.V. Functional reorganization of the default mode network across chronic pain conditions. *PLoS ONE* **2014**, *9*, e106133. [[CrossRef](#)] [[PubMed](#)]
119. Hwang, R.J.; Chen, L.F.; Yeh, T.C.; Tu, P.C.; Tu, C.H.; Hsieh, J.C. The resting frontal alpha asymmetry across the menstrual cycle: A magnetoencephalographic study. *Horm. Behav.* **2008**, *54*, 28–33. [[CrossRef](#)] [[PubMed](#)]
120. Hwang, R.J.; Wu, C.H.; Chen, L.F.; Yeh, T.C.; Hsieh, J.C. Female menstrual phases modulate human prefrontal asymmetry: A magnetoencephalographic study. *Horm. Behav.* **2009**, *55*, 203–209. [[CrossRef](#)] [[PubMed](#)]
121. Vachon-Presseau, E.; Roy, M.; Martel, M.O.; Caron, E.; Marin, M.F.; Chen, J.; Albouy, G.; Plante, I.; Sullivan, M.J.; Lupien, S.J.; et al. The stress model of chronic pain: Evidence from basal cortisol and hippocampal structure and function in humans. *Brain* **2013**, *136*, 815–827. [[CrossRef](#)] [[PubMed](#)]
122. Phillips, K.; Clauw, D. Central pain mechanisms in chronic pain states—maybe it is all in their head. *Best Pract. Res. Clin. Rheumatol.* **2011**, *25*, 141–154. [[CrossRef](#)] [[PubMed](#)]
123. Kuner, R.; Flor, H. Structural plasticity and reorganisation in chronic pain. *Nat. Rev. Neurosci.* **2016**, *18*, 20–30. [[CrossRef](#)] [[PubMed](#)]
124. Yen, C.T.; Lu, P.L. Thalamus and pain. *Acta Anaesthesiol. Taiwanica* **2013**, *51*, 73–80. [[CrossRef](#)] [[PubMed](#)]
125. Rainville, P.; Duncan, G.H.; Price, D.D.; Carrier, B.; Bushnell, M.C. Pain affect encoded in human anterior cingulate but not somatosensory cortex. *Science* **1997**, *277*, 968–971. [[CrossRef](#)] [[PubMed](#)]
126. Bushnell, M.C.; Čeko, M.; Low, L.A. Cognitive and emotional control of pain and its disruption in chronic pain. *Nat. Rev. Neurosci.* **2013**, *14*, 502–511. [[CrossRef](#)] [[PubMed](#)]
127. Liu, Q.; Chen, Y.F.; Fan, S.Z.; Abbod, M.F.; Shieh, J.S. EEG signals analysis using multiscale entropy for depth of anesthesia monitoring during surgery through artificial neural networks. *Comput. Math. Methods Med.* **2015**, *2015*, 1–16. [[CrossRef](#)] [[PubMed](#)]
128. Valencia, J.F.; Melia, U.S.P.; Vallverdú, M.; Borrat, X.; Jospin, M.; Jensen, E.W.; Porta, A.; Gambús, P.L.; Caminal, P. Assessment of nociceptive responsiveness levels during sedation-analgesia by entropy analysis of EEG. *Entropy* **2016**, *18*. [[CrossRef](#)]
129. Courtiol, J.; Perdakis, D.; Petkoski, S.; Müller, V.; Huys, R.; Sleimen-Malkoun, R.; Jirsa, V.K. The multiscale entropy: Guidelines for use and interpretation in brain signal analysis. *J. Neurosci. Methods* **2016**, *273*, 175–190. [[CrossRef](#)] [[PubMed](#)]
130. Ahmed, M.U.; Li, L.; Cao, J.; Mandic, D.P. Multivariate multiscale entropy for brain consciousness analysis. In Proceedings of the Annual International Conference of the IEEE Engineering in Medicine and Biology Society, EMBS, Boston, MA, USA, 6–18 June 2011; Volume 2011, pp. 810–813.

131. Dos Santos Pinheiro, E.S.; de Queirós, F.C.; Montoya, P.; Santos, C.L.; do Nascimento, M.A.; Ito, C.H.; Silva, M.; Nunes Santos, D.B.; Benevides, S.; Miranda, J.G.V.; et al. Electroencephalographic patterns in chronic pain: A systematic review of the literature. *PLoS ONE* **2016**, *11*, e0149085. [[CrossRef](#)]
132. Ploner, M.; Sorg, C.; Gross, J. Brain Rhythms of Pain. *Trends Cogn. Sci.* **2016**, *21*, 100–110. [[CrossRef](#)] [[PubMed](#)]
133. Nagarajan, R. Quantifying physiological data with Lempel-Ziv complexity—Certain issues. *IEEE Trans. Biomed. Eng.* **2002**, *49*, 1371–1373. [[CrossRef](#)] [[PubMed](#)]
134. Lapidoth, A.; Ziv, J. On the universality of the LZ-based decoding algorithm. *IEEE Trans. Inf. Theory* **1998**, *44*, 1746–1755. [[CrossRef](#)]
135. Zhang, X.S.; Roy, R.J.; Jensen, E.W. EEG complexity as a measure of depth of anesthesia for patients. *IEEE Trans. Biomed. Eng.* **2001**, *48*, 1424–1433. [[CrossRef](#)] [[PubMed](#)]



© 2017 by the authors. Licensee MDPI, Basel, Switzerland. This article is an open access article distributed under the terms and conditions of the Creative Commons Attribution (CC BY) license (<http://creativecommons.org/licenses/by/4.0/>).